1   **Dryland watersheds in flux: How nitrogen deposition and changing**

2   **precipitation regimes shape nitrogen export**

3   [1]Jianning Ren, [1]Erin J. Hanan, [2]Paolo D'Odorico, [3]Naomi Tague, [4]Joshua P. Schimel, [5]Peter M.

4   Homyak

5   [1]Department of Natural Resources and Environmental Science, University of Nevada, Reno,

6   89501, Reno, USA

7   [2]Department of Environmental Science, policy, & Management, University of California,

8   Berkeley, 94720, Berkely, USA

9   [3]Bren School of Environmental Science & Management, University of California, Santa Barbara,

10   93106, Santa Barbara, USA

11   [4]Department of Ecology, Evolution and Marine Biology, University of California, Santa Barbara,

12   93106, Santa Barbara, USA

13   [5]Department of Environmental Sciences, University of California, Riverside, 92521, Riverside,

14   USA

15

16

17   Correspondence:

18   Jianning Ren (nren@unr.edu, renjianning@gmail.com)

19   Erin Hanan (ehanan@unr.edu)

20

Abstract

Atmospheric nitrogen (N) deposition and climate change are transforming the way N moves through dryland watersheds. For example, N deposition is increasing N export to streams, which may be exacerbated by changes in the magnitude, timing, and intensity of precipitation (i.e., the precipitation regime). While deposition controls the amount of N entering a watershed, the precipitation regime influences rates of internal cycling; when and where soil N, plant roots, and microbes are hydrologically connected; how quickly plants and microbes assimilate N; and rates of denitrification, runoff, and leaching. We used the ecohydrological model RHESSys to investigate (1) how N dynamics differ between N-limited and N-saturated conditions in a dryland watershed, and (2) how total precipitation and its intra-annual intermittency (i.e., the time between storms in a year), interannual intermittency (i.e., the duration of dry months across multiple years), and interannual variability (i.e., variance in the amount of precipitation among years) modify N dynamics. Streamflow N export was more sensitive to increasing intermittency and variability in N-limited vs. N-saturated model scenarios, particularly when total precipitation was lower—the opposite was true for denitrification. N export and denitrification increased or decreased the most with increasing interannual intermittency compared to other changes in precipitation amount. This suggests that under future climate change, prolonged droughts that are followed by more intense storms may pose a major threat to water quality in dryland watersheds.

Key points:

- We developed a new metric for identifying when a dryland watershed becomes "capacity N-saturated".
- Streamflow N export was more sensitive to precipitation regime changes in N-limited than N-saturated watersheds.

44 • N export increased or decreased the most with increasing interannual intermittency than

45 other changes in precipitation amount.

46 **1 Introduction**

47 Atmospheric N deposition has been increasing in dryland watersheds of the western US

48 since the 1860s, largely due to human population growth and concomitant increases in both

49 fossil fuel consumption and industrial agriculture (Galloway et al., 2008; Kanakidou et al.,

50 2016). In many populated regions around the globe, N deposition is already around 20 times

51 higher than the natural rate of 0.05 g N g m^{-2} year^{-1} (Dentener et al., 2006; Galloway et al.,

52 2008). For example, in dryland chaparral watersheds near Los Angeles, California, the N

53 deposition rate is more than 3 g N m^{-2} year^{-1} (Benish et al., 2022). By 2050, rates are likely to

54 reach 5 g N m^{-2} year^{-1} (Sutton et al., 2007). Given these dramatic increases in N inputs, there is

55 an urgent need to understand (1) the point at which dryland watersheds will no longer be able to

56 assimilate additional N (i.e., the threshold of N deposition at which they become N-saturated)

57 and (2) how deposited N will be transformed and exported from watersheds through both

58 hydrologic and gaseous pathways (i.e., denitrification) under both N saturated and unsaturated

59 conditions. Precipitation plays an important role in driving N cycling, uptake, and export.

60 However, in drylands, these processes can act on different timescales and high precipitation

61 variability can complicate our ability to predict the fate of atmospherically deposited N (Homyak

62 et al., 2014; Howarth et al., 2006; Krichels et al., 2022; Ren et al., 2023, submitted).

63 Conceptual models used to assess N saturation and N export were developed in temperate

64 systems where relatively high and consistent rainfall maintains hydrologically connected soils

65 throughout the year, allowing substrates to diffuse to plant roots and be taken up (Homyak et al.,

66 2014). As a result, these models assume that N export occurs once a watershed exceeds the

67 capacity of plants and other ecosystem components to assimilate N and becomes N-saturated

68 (Aber et al., 1989). In drylands however, summer aridity can keep soils dry for months without

69 rain, limiting subsurface N transport and allowing it to accumulate in hydrologically

70 disconnected microsites (i.e., hotspots; Parker & Schimel, 2011). At the onset of the wet season

71 when rains return, N can be rapidly exported before plants and soil microbes can assimilate it—

72 this can produce large stream N losses (known as "pulses") that under traditional conceptual

73 models would suggest N saturation (Zhu et al., 2018). However, such hydrologic losses regularly

74 occur in drylands even when plants remain N-limited (Homyak et al., 2014).

75   To better account for asynchronies between N availability and uptake, Lovett & Goodale.

76 (2011) introduced the concept of **kinetic** N saturation, where available N can exceed demand

77 over short timescales (e.g., when a storm follows a long dry period). This contrasts with **capacity**

78 N-saturation, where an ecosystem or watershed can no longer assimilate N over longer

79 timescales, resulting in consistent increases in N export that correspond with increasing

80 atmospheric N inputs. Because both N saturation statuses can increase N export, it is difficult to

81 identify the threshold at which dryland watersheds shift from kinetic to capacity saturation. As a

82 result, it also remains difficult to predict the fate of atmospherically deposited N and how it

83 changes along a gradient from kinetic to capacity saturation.

84   Further complicating our understanding of N saturation and export, general circulation

85 models project changes in the both the total amount and timing of precipitation in drylands

86 (Fischer et al., 2013). These changes can occur on both intra- and interannual scales (Knapp et

87 al., 2002; Trenberth et al., 2003). On intra-annual time scales, a higher water-holding capacity in

88 a warming atmosphere can give rise to larger precipitation events with longer dry periods

89 between storms (i.e., higher *intra-annual intermittency*, Allen & Ingram, 2002). At interannual

90   scales, climate change can alter atmospheric circulation and moisture transport to promote

91   extreme wet months with a longer duration of dry months across multiple years (i.e., higher

92   *interannual intermittency* (Allen & Ingram, 2002; Trenberth et al., 2003). Alternatively, some

93   models project that climate change will enhance *interannual variability*, making dry years drier

94   and wet years wetter, while still retaining the intra-annual storm event characteristics (Pörtner et

95   al., 2022). Higher precipitation intermittency and variability can both affect N export, but

96   increases in intermittency, which change both the timing and magnitude of storms (i.e., fewer,

97   more intense storms), may have a different effect than changes in variability alone (which only

98   influences storm size without changing timing (Homyak et al., 2017; Winter et al., 2023). Recent

99   studies have shown that enhanced precipitation variability and intermittency can increase both

100   nitric oxide (NO) emissions and stream N export (Krichels et al., 2022; Winter et al., 2023),

101   however, most of these studies are event-based and the long-term, and cumulative effects of

102   altered precipitation regimes and their interactions with N deposition remain poorly understood.

103   A simulation modeling approach should be useful for identifying the threshold of

104   atmospheric N deposition at which a watershed transitions from kinetic to capacity saturation,

105   which would enable us to better project future N export. With this approach, we can directly

106   investigate how N export responds to temporal asynchrony between N availability and uptake;

107   for example, when the first rain event of a wet season flushes N while plants are not actively

108   growing (in a Mediterranean climate) vs. when the activation of rainy season overlaps with the

109   peak growing season in early spring (in a continental climate). We expect that when a watershed

110   only experiences kinetic saturation, there will be pronounced differences between these two

111   scenarios. Conversely, when a watershed is capacity N-saturated due to high N-deposition, total

112   N export will not change in response to the timing of precipitation.

113   Using a simulation modeling approach, we developed and tested our proposed metric for

114   identifying when a dryland watershed becomes "capacity N-saturated." Then using the new

115   metric, we developed N-limited and N-saturated scenarios to address two questions: (1) How do

116   changes in the precipitation regime, including the total amount of precipitation, its intra-annual

117   intermittency, interannual intermittency, and interannual variability influence watershed-scale N

118   export, and (2) How do these responses differ between N-limited and N-saturated watersheds?

119   These scenarios were conducted using the coupled ecohydrological-biogeochemical model

120   RHESSys (Tague & Band, 2004) in a dryland, chaparral-dominated watershed downwind of Los

121   Angeles, California that experiences high rates of N-deposition.

122   **2 Methods**

123   **2.1 Study site**

124   We developed modeling scenarios for the chaparral-dominated Bell 4 watershed in the

125   San Dimas Experimental Forest, located 50 km northeast of Los Angeles, California (34°12′N,

126   117°47′W). This is a small watershed (0.14 km^2) with elevations ranging from 700 to 1024

127   meters. The soils are shallow, coarse-textured sandy loams weathered from granitic parent

128   material (Chaney et al., 2016; Dunn et al., 1988); they classify as Typic or Lithic Xerorthents

129   (Hubbert et al., 2006; Ryan, 1991). The climate is characterized by hot and dry summers and

130   cool-humid winters. Mean annual precipitation is approximately 700 mm, with daily

131   temperatures ranging from -8°C in winter to 40 °C in summer. Vegetation on south-facing slopes

132   includes chamise (*Adenostoma fasciculatum*), California lilac (*Ceanothus spp.*), and black sage

133   (*Salvia mellifera*), while north-facing slopes are covered by *ceanothus spp.* and California laurel

134   (*Umbellularia californica*). Riparian areas are dominated by live oak (*Quercus agrifolia*). Being

135   downwind from a major metropolitan area, Bell 4 experiences high N deposition rates, which

136   exceed 30 kg ha^{-1} year^{-1} (Benish et al., 2022; Bytnerowicz & Fenn, 1996).

137   **2.2 RHESSys model**

138   To investigate how precipitation regime changes affect N cycling and export in drylands

139   and how they are different between N-limited and N-saturated watersheds, we used the regional

140   hydro-ecologic simulation system (RHESSys). RHESSys is a spatially distributed model that

141   fully couples hydrological processes with biogeochemical processes, allowing it to simulate the

142   effects of climate and environmental change on C and N cycling and hydrologic conditions

143   (Garcia et al., 2016; Lin et al., 2015; Tague & Band, 2004). Recent model improvements have

144   enabled RHESSys to better-represent N cycling and transport in dryland watersheds (Burke et

145   al., 2021; Hanan et al., 2017, Ren et al., 2023, submitted). This includes refining nitrification

146   processes after wildfire in chaparral (Hanan et al., 2017), and representing biogeochemical

147   hotspots explicitly across a landscape (Ren et al., 2023, submitted). RHESSys has been

148   extensively evaluated in several dryland watersheds across the western US (Burke et al., 2021;

149   Chen et al., 2020; E. S. Garcia & Tague, 2015; Elizabeth S. Garcia et al., 2016; Hanan et al.,

150   2017, 2021; Ren et al., 2021, 2022; Reyes et al., 2017; Stephens et al., 2022).

151   C and N cycling among vegetation, litter, and soil layers are simulated at a patch scale

152   (the smallest spatial unit; 3-meter resolution in this study). Photosynthesis is calculated using the

153   Farquhar model which is a function of stomatal conductance, radiation, nitrogen and carbon

154   dioxide concentration, air temperature and atmospheric pressure (Farquhar & von Caemmerer,

155   1982). Plant respiration includes maintenance and growth respiration, which is estimated using

156   Ryan. (1991) model. Carbon is then allocated to roots, stems, and leaves using an architecture (or

157   age) based method (Dickinson et al., 1998). RHESSys has four litter pools and four soil pools

158   with different C:N ratios and decomposition rates. Decomposition is estimated based on a

159   defined maximum decomposition rate and constrained by soil moisture, soil temperature, and

160   nitrogen availability. N mineralization and immobilization are estimated using the C:N ratios of

161   the litter and soil pools when materials decompose from one pool to another (Hanan et al., 2017;

162   Tague & Band, 2004).

163   RHESSys calculates nitrification rates based on the CENTURY$_{NGAS}$ model which is a

164   function of soil pH, soil moisture, soil temperature, and available soil ammonium (Parton, 1996).

165   A maximum denitrification rate is calculated as a function of the total available nitrate (NO_3^-) in

166   soil, and total soil carbon and nitrogen, and then the maximum rate is modified based on soil

167   moisture and soil respiration as a proxy for microbial abundance.

168   Soil moisture processes include four vertical layers, a surface detention store, a root zone

169   store, an unsaturated store, and a saturated store. At a daily timestep, the surface detention store

170   receives water from canopy throughfall and snowmelt (when present), and infiltrates into the soil

171   based on the Phillip (1957) infiltration equation. Overland flow is generated when the ponded

172   water is above the detention storage capacity. Water can percolate into a deeper ground water

173   store through bypass flow. Water drains from the unsaturated zone or root zone to the saturated

174   zone based on hydraulic conductivity and moves from the saturated zone to the unsaturated zone

175   or root zone based on the Eagleson (1978) equation. Subsurface lateral flow between patches

176   follows topographic gradients and soil hydraulic parameters such as saturation deficit and

177   transmissivity. N moves with these water fluxes based on its concentration (Tague & Band,

178   2004). Atmospherically deposited N enters the soil through infiltration from the surface

179   detention store. In the unsaturated zone, soil nitrate decreases exponentially with depth. In the

180   saturated zone, nitrate export follows a flushing hypothesis, where more soil N becomes

181   available for flushing to streams as the water table rises (Chen et al., 2020).

182   To account for sub-grid scale heterogeneity in vegetation cover, RHESSys can be run

183   using a new aspatial framework (Burke et al., 2021). In this new framework, "patch families" are

184   the smallest spatially explicit model unit, and "aspatial patches" nested within a patch family are

185   the smallest aspatial model unit. Aspatial patches do not have physical locations, but instead

186   represent a distribution of vegetation types based on observed or hypothetical distributions.

187   Local routing of water between aspatial patches within a patch family is based on the relative

188   moisture differences among aspatial patches in the rooting and unsaturated zones and mediated

189   by user-defined gaining and losing coefficients for each patch type (Burke et al., 2021). Local

190   routing in the saturated zone is based on the differences in the groundwater table and it carries

191   nitrate when exchanging water.

192   We also recently expanded the aspatial patch framework to incorporate the role of fine-

193   scale biogeochemical "hotspots," represented as aspatial patches within each patch family—

194   these represent a distribution of microsites (e.g., soil aggregates) where biogeochemical cycling

195   can be hydrologically disconnected, as soils dry out, from other aspatial patches that contain

196   plant roots (Ren et al. 2023, submitted). Hotspots help drive kinetic N saturation by enabling N

197   to accumulate and subsequently be flushed from the system when soils are rewetted.-To model

198   hotspot dynamics, the framework includes: (1) model algorithms that enable hotspots to access

199   soil and litter C and N from neighboring non-hotspot patches for decomposition and

200   biogeochemical cycling, and (2) algorithms and parameters that control the moisture conditions

201   under which hotspots are hydrologically disconnected from other aspatial patches in the saturated

202   zone, (3) parameters that control water diffusion in the unsaturated and/or root zone between

203   hotspot and non-hotspot patches as soils dry out. For detailed descriptions of the RHESSys

204   model and the new hotspot framework, refer to Tague & Band, (2004) and Ren. et al (2023,

205   under review).

206   **2.3 Data**

207   To represent topography across the watershed, we used a 1-meter resolution digital

208   elevation model (DEM) from LiDAR aggregated to 10-meters (Ren et al., 2023, submitted). Soil

209   texture was delineated across the watershed using the POLARIS database (Chaney et al., 2016).

210   To map landcover across Bell 4, we aggregated 1-meter resolution land cover data from the

211   National Agriculture Imagery Program (NAIP; collected on June 5, 2016) to 3-meters. We then

212   classified three land cover types across the watershed: chaparral, live oak, and bare ground

213   (Maxwell et al., 2017). RHESSys patch families were established based on the 10-meter DEM,

214   while the aspatial patch vegetation distributions were classified based on the 3-meter NAIP data

215   (Ren et al., 2023, submitted). The Bell 4 basin contained 1259 patch families, with each patch

216   family having approximately 11 aspatial patches. We acquired meteorological forcing data from

217   1979 to 2020 from the gridMET, including daily maximum and minimum temperatures,

218   precipitation, relative humidity, radiation, and wind speed (Abatzoglou, 2013). Daily streamflow

219   data from 1980 to 2002 and stream N data from 1988 to 2000 were provided by U.S. Forest

220   Service (USFS).

221   **2.4 Model initialization and calibration**

222   To initialize soil C and N pools to steady state, we spun RHESSys up for three hundred

223   years. Then to initialize vegetation C and N pools, we used a target-driven spin-up approach,

224   which leverages remotely sensed LAI calculated from NAIP (at April 24, 2010) to set target

225   values for each patch across the watershed; this enables us to spin the model up mechanistically

226   while still capturing landscape heterogeneity (Hanan et al., 2018). We then calibrated six soil

227   parameters using observed streamflow data: saturated hydraulic conductivity (K_{sat}), the decay of

228   K_{sat} with depth (m), pore size index (b), air entry pressure (ϕ), bypass flow to deeper

229   groundwater storage (gw_1), and deep groundwater drainage rates to stream (gw_2). We selected

230   the best parameters by comparing the observed and modeled streamflow using the monthly

231   Nash-Sutcliffe efficiency (NSE; Nash & Sutcliffe, 1970) and percent error of annual streamflow.

232   We used eight years of streamflow data from 1993 to 2002 for calibration and three years from

233   1980 to 1983 for validation. Following calibration, we designated one aspatial patch in each

234   patch family to represent hotspots, assuming that hotspots were evenly distributed across the

235   landscape. We then optimized the hotspot-related parameters (i.e., the water sharing coefficient

236   between aspatial patches and subsurface flow threshold) by comparing modeled and observed

237   streamflow N from 1988 to 2000. During the calibration, the monthly NSE of simulated

238   streamflow reached 0.88 with a percent error of 5.45%, while for the validation period, the

239   monthly NSE was 0.80 with a percent error of -3.92%. This suggests a close match between

240   modeled and measured streamflow timing and volume. By including hotspots in the model, we

241   also improved our ability to capture the timing of peak streamflow nitrate observations (NSE =

242   0.40). A more detailed description of initialization and calibration results can be found in Ren et

243   al. (2023, submitted).

244   **2.4 Scenarios**

245   2.4.1 Developing better metrics for N-saturation in dryland watersheds.

246   Because seasonal N export to streams is characteristic in dryland watersheds, even when

247   they are not N-polluted (Homyak et al., 2014), we need to develop metrics that can identify when

248   a watershed shifts from kinetic to capacity saturation (Lovett & Goodale, 2011). This requires

249   understanding how N deposition interacts with the timing of precipitation. To determine the N

250   deposition threshold at which a watershed becomes N-saturated, we built scenarios considering

251   interactions between the N deposition rate and precipitation seasonality over a period of 60

252   years. Because the observed meteorological forcing data spans only 40 years (water years 1980

253   to 2020), we repeated this data to construct the additional 20 years. This included three scenarios

254   for precipitation seasonality: a dry summer scenario (to match observations), a wet summer

255   scenario (to represent a more continental climate), and an evenly distributed scenario (Figure 1a).

256   The wet summer and evenly distributed scenarios were reconstructed from the observed

257   precipitation data by manipulating the duration of dry days and the timing of precipitation using

258   a method from Rodriguez-Iturbe et al. (1999) which will be introduced in detail in section 2.4.2.

259   We also included 12 dry N deposition scenarios (including 0.05, 0.25, and 0.5 to 5 g m^{-2} year^{-1} at

260   an increment of 0.5 g m^{-2} year^{-1}). This resulted in 36 scenarios for precipitation and N deposition

261   in a factorial design.

262   To determine the level of N deposition at which our watershed becomes N-saturated, we

263   examined N export for each scenario and determined the magnitude of N deposition where

264   export no longer varied under different precipitation seasonality scenarios. This approach

265   assumes that under kinetic saturation, dry summers would promote more N export because

266   rainfall occurs when plants are less active. We define the N deposition threshold above which the

267   watershed is capacity N saturated as the amount of N deposition required for mean normalized

268   streamflow N (i.e., annual streamflow N divided by the N deposition rate) in both the dry

269   summer and the evenly distributed scenarios to be above 90% of the mean normalized

270   streamflow in the dry winter scenario. Using this threshold, we then built two scenarios for N

271   saturation status: N-saturated and N-limited. This involved scaling N deposition up or down such

272   that the N saturated scenario had 100 times higher N deposition than the N-limited scenario. We

273   then used these scenarios for the following sensitivity analysis to examine how precipitation

274   intermittency and variability influence N export under saturated and unsaturated conditions.

275   2.4.2 Effects of intra-annual precipitation intermittency on N export

276   To understand the how intra-annual precipitation intermittency influence N export, we

277   used a stochastic precipitation generator, based on Rodriguez-Iturbe et al. (1999). Within a given

278   year, the occurrence and amount of total daily precipitation can be viewed as a stochastic

279   process. Specifically, the occurrence of rainfall is modeled as a **Poisson process with a rate λ**

280   **(average rainfall frequency)**, and the amount of rainfall for each event is determined by a

281   random exponential distribution. As our model operates on a daily timestep, we did not consider

282   the temporal structure of rainfall within each event and instead assumed the precipitation

283   occurred instantaneously.

284   Based on these assumptions, the distribution of the length of dry days (τ) between precipitation

285   events is an exponential distribution with a mean $1/\lambda$ (the unit of λ is 1/day).

286    $$f_\tau(\tau) = \lambda\, e^{-\lambda\tau},\ for\ \tau \geq 0 \qquad\qquad \text{Eq (1)}$$

287   The amount of precipitation is an independent random variable *h (mm/day)*, calculated by an

288   exponential probability density function:

289    $$f_H(h) = \frac{1}{\alpha}e^{-\frac{h}{\alpha}},\ for\ h \geq 0 \qquad\qquad \text{Eq (2)}$$

290   Where α is the mean of daily rainfall amount (mm/day) when precipitation occurs for a certain

291   year and can be estimated from the observed data.

292   The total amount of precipitation R (mm year^{-1}) for a given year can therefore be calculated as

293    $R = h \times T/\tau$ Eq (3)

294   Where T is the total days for a rainy season.

295   We estimated the two parameters (λ_0 and α) for the stochastic model based on observed

296   precipitation. Then we adjusted the rainfall frequency parameter $1/\lambda\_0$ by a factor of 2 to 4 to

297   increase the duration of dry days between rainfall events. Additionally, we adjusted the mean

298   daily rainfall amount α to maintain consistent total precipitation amounts across different

299   scenarios. In total, we developed five distinct intra-annual intermittency scenarios (Figure 1b).

300   To summarize, within one year, this method determines the number of dry days across a

301   rainy season and uses rainfall intensity and the number of days with precipitation (from

302   observations) to determine the size and timing of storms that occur between dry days. This

303   enables us to vary rainfall intermittency, while maintaining a fixed amount of precipitation for

304   each year. Then, to examine how precipitation intermittency interacts with the total amount of

305   precipitation (e.g., under drier vs. wetter futures), we developed five precipitation scalers for

306   each intermittency scenario (ranging from 0.6 to 1.4 at an increment of 0.2). Hereafter, we refer

307   to scenarios with precipitation scaling factors less than one as "drier future" scenarios and greater

308   than one as "wetter future" scenarios. By combing five precipitation scaling factor scenarios,

309   two N saturation scenarios, and five intra-annual intermittency scenarios, we generated a total of

310   40 different scenarios in a factorial design and ran the model for 60 years (Figure 2).

311   2.4.3 The effect of interannual intermittency on N export

312   To investigate the effects of interannual precipitation intermittency on N export, we used

313   a stochastic precipitation generator that was similar to the one used for the intra-annual

314   precipitation intermittency analysis. Specifically, we examined monthly precipitation data for a

315   period of 40 years (in total 480 months) and modeled both the amount of monthly precipitation

316   and duration of dry months as stochastic processes. We initially ignored the temporal structure of

317   precipitation within each month and calculated the two parameters λ_0 (unit is 1/month) and α

318   (mm/month). We then downscaled the modeled monthly precipitation to a daily timestep based

319   on observed precipitation considering the temporal structure of rainfall events within a month.

320   To increase the interannual intermittency, we then manipulate the two parameters (λ and α) to

321   increase both the duration and the mean amount of monthly precipitation while maintaining

322   consistent total precipitation levels over the 40-year period (Figure 1d). Again, we built 40

323   scenarios by combining the five interannual intermittency scenarios with the previous four

324   precipitation scaling factors and the two N saturation scenarios and ran RHESSys for 60 years by

325   looping the 40 years reconstructed data.

326   2.4.4 Effect of interannual precipitation variability on N export

327   To understand the effects of interannual precipitation variability on N export, we adapted

328   methodology proposed by Gherardi & Sala (2015). We generated different scenarios for

329   interannual precipitation variability by manipulating the observed precipitation data. To increase

330   variability, we increased the annual precipitation amount in wet years and decreased it in dry

331   years (by 20%, 40%, 60% relative to the observed amounts). To decrease variability, we lessened

332   the amount of annual precipitation in wet years and increased it in dry years (by 20%, 40%, 60%

333   and 80%). This approach enabled us to create scenarios with varying coefficients of variation

334   (CV) while keeping the total precipitation the same throughout the simulation period. This

335   resulted in eight interannual variability scenarios including a baseline scenario (Figure 1c). By

336   combing them with five total precipitation scaling factors, and two levels of N saturation (N-

337   limited vs. N-saturated), we generated 80 factorial scenarios.

338
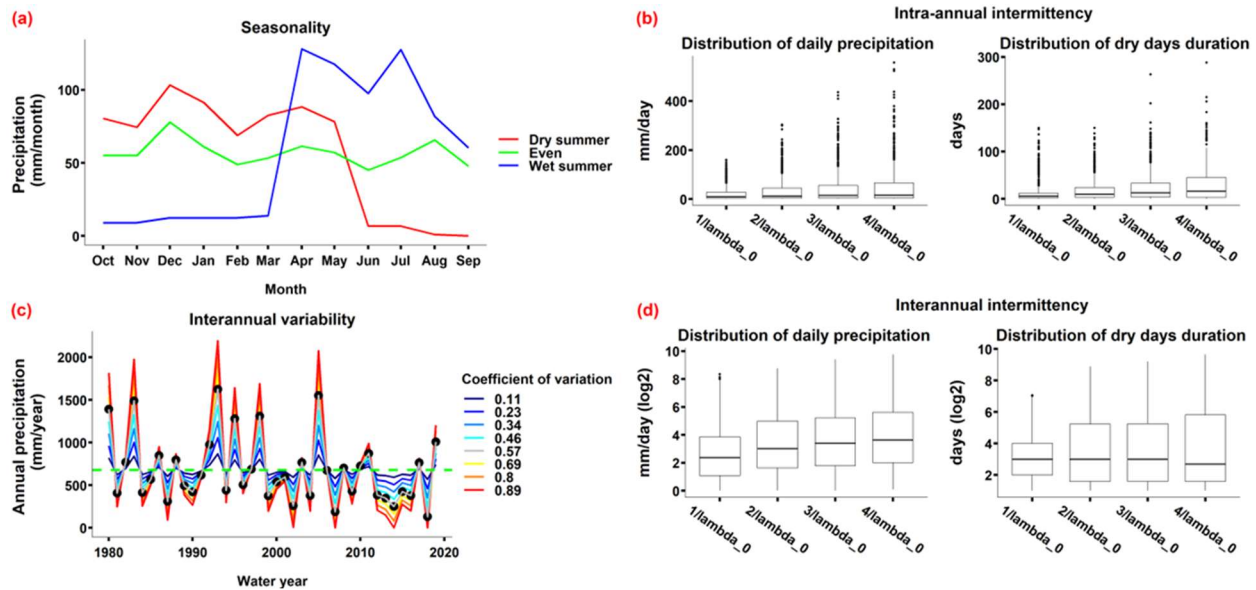
Figure 1. A summary of reconstructed precipitation data used. Panel a represents the precipitation seasonality scenarios: dry summer, evenly distributed across the year, and wet summer. The dry summer scenarios used observed precipitation data. Total precipitation and inter-annual intermittency over the 40 years was consistent across three scenarios. Panel b represents the reconstructed precipitation data with different intra-annual intermittencies for a period of 40 years, including the distribution of daily precipitation and dry days duration. The total amount of precipitation over 40 years was the same for all four precipitation intermittency scenarios. Lambda (λ_0) is the frequency of observed rain events, and the x-axis shows an increase in intermittency. The comparison between observed and reconstructed precipitation of $1/\lambda\_0$ is shown in Figure S1. Panel c represents reconstructed and observed precipitation for different levels of interannual variability. The green horizontal line is the mean annual precipitation from the observation data and the black dots are the observed annual precipitation. Blue lines correspond with lower variability relative to observation, red lines correspond with higher variability relative to observation. Panel d represents reconstructed precipitation data with different interannual intermittencies for a period of 40 years, including the distribution of daily precipitation amounts and the distribution of duration of dry days. The total amount of precipitation over 40 years was the same for all five precipitation scenarios at a given precipitation scaling factor. Lambda (λ_0) is the frequency of reconstructed baseline rain events, and the x-axis shows an increase in intermittency. Note that the y axis is in $\log_2$ scale to better show extreme values.

To summarize, we developed two scenarios for N saturation status (N-saturated vs N-limited), five precipitation scaling factors (0.6, 0.8, 1, 1.2, 1.4), and three sets of scenarios for changes in precipitation timing. These changes include four intra-annual intermittency scenarios, four interannual intermittency scenarios, and eight interannual variability scenarios. This resulted

363   in 160 factorial scenarios (Figure 2). We then calculated the normalized differences in N fluxes

364   for each precipitation regime relative to its baseline, defined as the lowest variability or

365   intermittency scenario for each precipitation scaling factor and N saturation status. For example,

366   in the N-limited scenarios, to compare N export among intra-annual intermittency scenarios at a

367   given precipitation scaling factor, we calculated differences between a given intermittency

368   scenario and the baseline ($1/\lambda\_0$). This resulted in 5 baseline intermittency scenarios (two drier,

369   two wetter, and a scenario with the baseline precipitation variability and total amount). The

370   combination of high precipitation scaling factors and high intermittency/variability can interact

371   to create some extreme storms that are historically unprecedented, though within the range of

372   possible future projections (Knapp et al., 2015). However, median storm sizes are well within the

373   range of historical variability for these semiarid systems; we focus on median values in our

374   discussion.
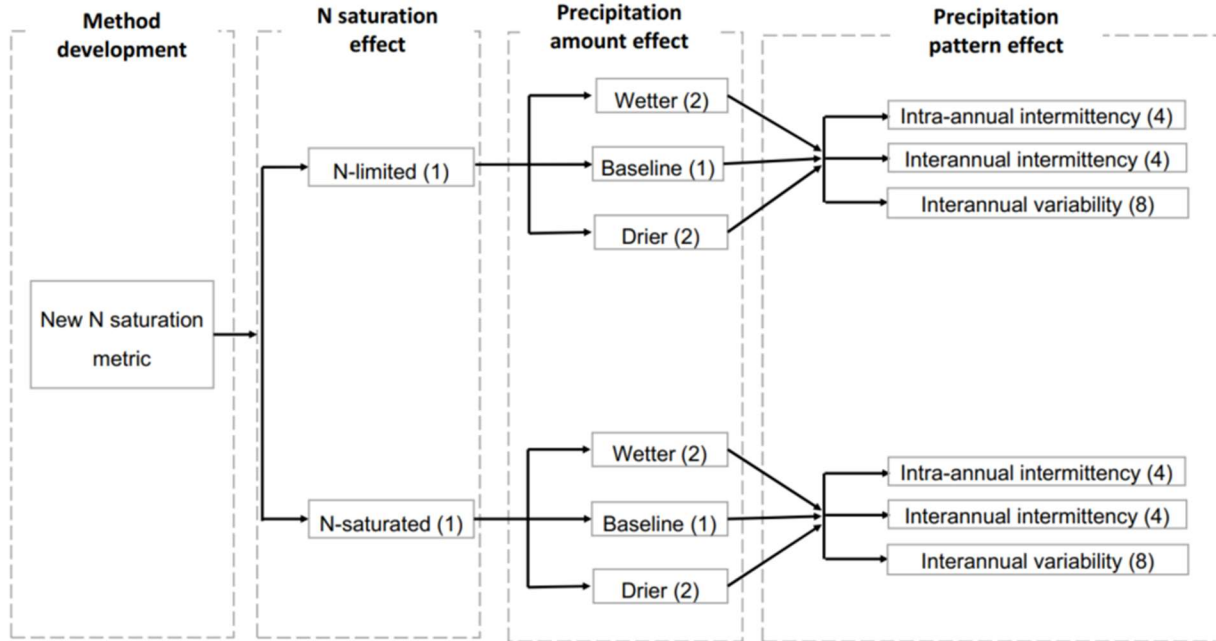
Figure 2. Summary of the scenarios developed to examine how interactions between N deposition and changes in precipitation regime affect N export. The number inside the parenthesis indicates the number of corresponding scenarios.

3 Results

3.1 A better metric for N saturation in drylands

In scenarios with relatively low atmospheric N deposition (i.e., smaller than 1 g m^{-2} year^{-1}), the mean and distribution of annual streamflow N (over 60 years) varied depending on the seasonality of precipitation, with the dry summer scenario resulting in the highest export and the wet summer scenario resulting in the lowest (Figure 3 and Figure S2). However, as N deposition increased, the watershed became less N-limited, leading to similar mean values and streamflow N distributions across different precipitation seasonality scenarios. This can be attributed to the fact that in a watershed with dry summers, the wet winter period can flush N to streams before plants begin to take it up, whereas in watersheds with wet summers, N is consumed by plants prior to leaching, resulting in less streamflow N export. Consequently, it can be inferred that

18

390   when the watershed is N-limited, the dry summer scenario would yield higher streamflow N

391   export than the dry winter scenario. Conversely, in an N-saturated watershed, the consumption of

392   N by plants and microbes would have a much smaller effect on streamflow N export. Using this

393   logic, we identify an N deposition threshold of approximately 2 g m^{-2} year^{-1} above which the

394   watershed becomes N-saturated. At this threshold, the ratio of the normalized mean annual

395   streamflow N for the wet summer:dry summer scenarios was no smaller than 0.9 (the same was

396   true for the evenly distributed scenario; Figure 3). For the following scenarios, we selected 0.05

397   g m^{-2} year^{-1} and 5 g m^{-2} year^{-1} to represent extremes of N-limited and N-saturated systems,

398   respectively.

399
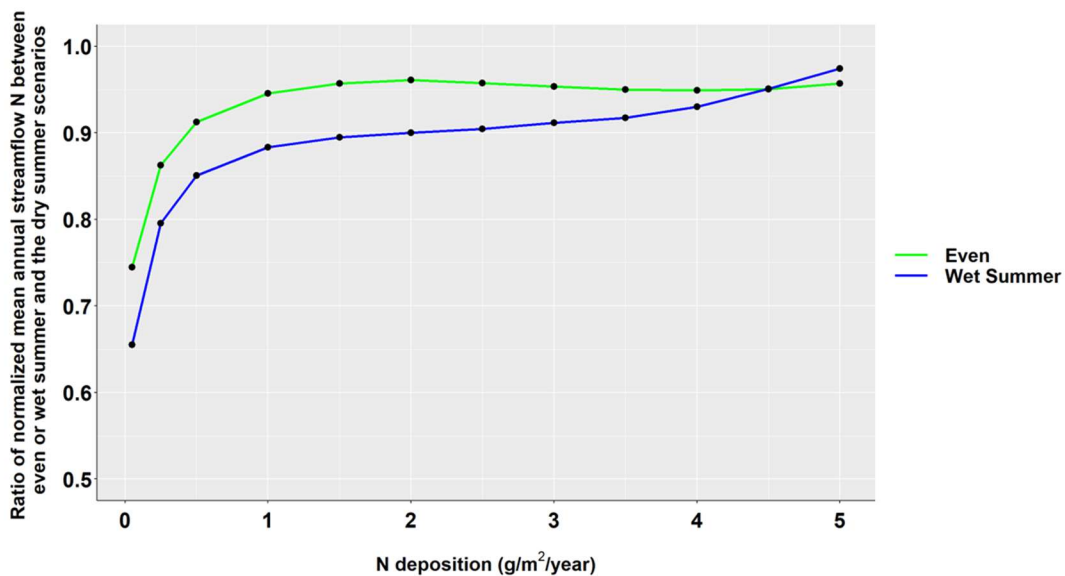
Figure 3. Ratio of the normalized mean annual streamflow N export between scenarios
(calculated as wet summer/dry summer (blue line) or even/dry summer (green line); values are
normalized by the N deposition rate). We selected an N saturated threshold where normalized
streamflow N in the wet summer scenario was no smaller than 90% of that observed in the dry
summer scenario. We used mean, rather than median values to account for extreme values.

3.2 The effect of changing precipitation regimes on N export.

3.2.1 The effect of intra-annual precipitation intermittency on N export.

Streamflow N export increased with higher intra-annual intermittency, which alters both the timing and magnitude of storms (Figure 4). Moreover, in N-limited scenarios, a higher total precipitation scaling factor generally increased streamflow N export (Figure 4). However, in N-saturated scenarios, baseline conditions can lead to more streamflow N export (Figure 4a). Higher intermittency implies longer dry periods and greater differences in precipitation amount between dry and wet periods, despite the same total precipitation among scenarios over the 60-year simulation. This can increase soil N accumulation during dry periods while reducing denitrification and N uptake (model estimates of plant carbon declined from 6 kg m^{-2} to around 4 kg m^{-2} between the highest and lowest intermittency scenario, Figure S4b). As a result, more N is flushed to streams during the wet periods. For both N-limited and N-saturated scenarios, denitrification decreased with higher levels of intermittency (Figure 4 b and e), primarily due to slower rates of decomposition caused by decreases in plant growth and litter production (Figure S4a).
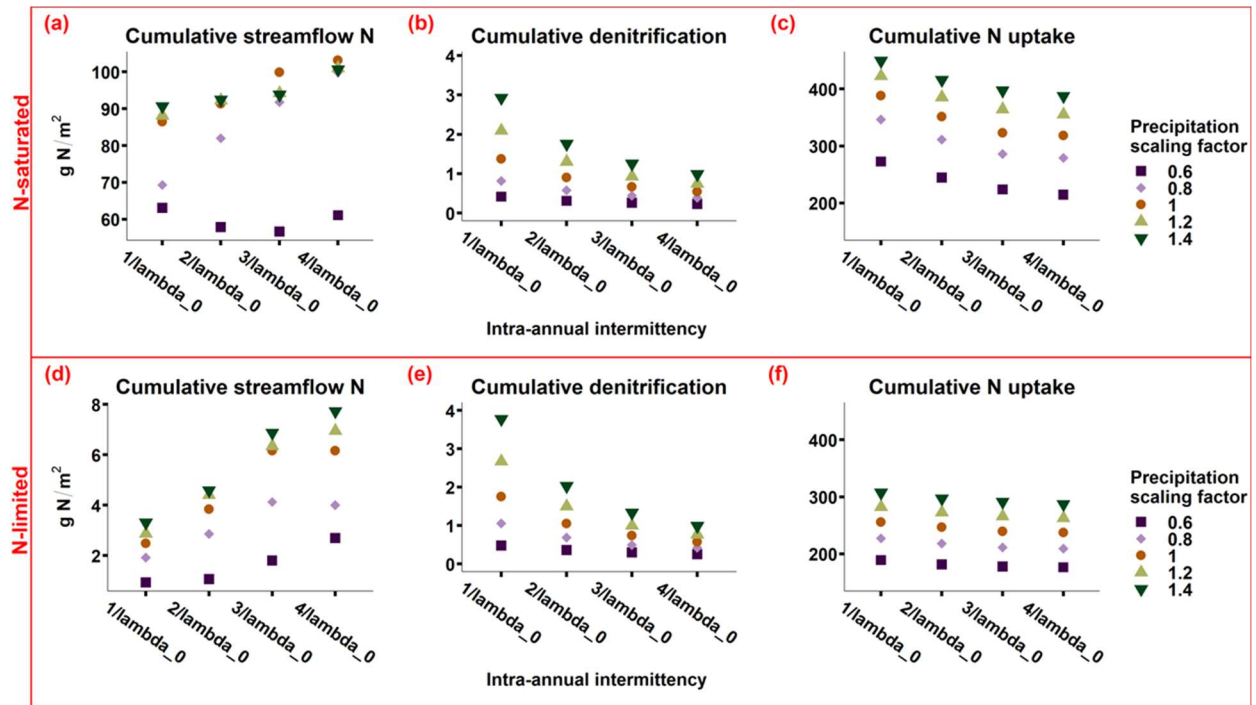
Figure 4. Sensitivity of cumulative N fluxes over 60 years (absolute value) to intra-annual precipitation intermittency for N-saturated and N-limited scenarios. The x axis is the duration of dry days between rainfall event, larger values represent higher intra-annual intermittencies.

Streamflow N export and denitrification were more sensitive to intra-annual precipitation intermittency in N-limited scenarios than in N-saturated scenarios, while plant N uptake was more sensitive to intra-annual intermittency in N saturated scenarios (Figure 5). For example, plant C declined 12% (from 3.9 to 3.4 kg m^{-2}) in N-limited scenarios but declined 27.5% (from 5.8 to 4.2 kg m^{-2}) in N-saturated ones (Figure S4a). The declines in plant carbon with higher intra-annual intermittency were smaller in N-limited scenarios because plants can be limited by both N and water, and changing water availability does not matter as much in N-limited as it does in N saturated scenarios, where once N limitation was alleviated, vegetation growth became more limited by water availability. In addition, streamflow N export increased with higher levels of intra-annual intermittency, while denitrification decreased (Figure 5a, b). This suggests

21

434   increases in intra-annual intermittency can increase N export to streams while decreasing N

435   losses to the atmosphere.

436   In N-saturated scenarios, streamflow N export was most sensitive to variation in intra-

437   annual intermittency under a precipitation scaling factor of 0.8, while in N-limited scenarios,

438   scaling factors of 0.6 or 1 were the most sensitive (Figure 5a, b). In N-limited scenarios, the 0.6

439   scaling factor showed the strongest exponential increases in streamflow N export with increasing

440   intermittency, indicating that the drier future scenarios have the largest sensitivity to

441   intermittency changes.

442   Denitrification in the wetter future scenarios decreased more with increasing intra-annual

443   precipitation variability than in the drier future scenarios because total denitrification was higher

444   in wetter baseline intermittency scenarios ($1/\lambda\_0$). With greater intra-annual intermittency, these

445   decreases were larger (Figure 5b, e). By contrast, in dry scenarios, plant N uptake decreased

446   slightly more with increasing intra-annual intermittency than in wetter scenarios, but the

447   magnitude was relatively small compared to streamflow N export and denitrification ((Figure 5c,

448   f).
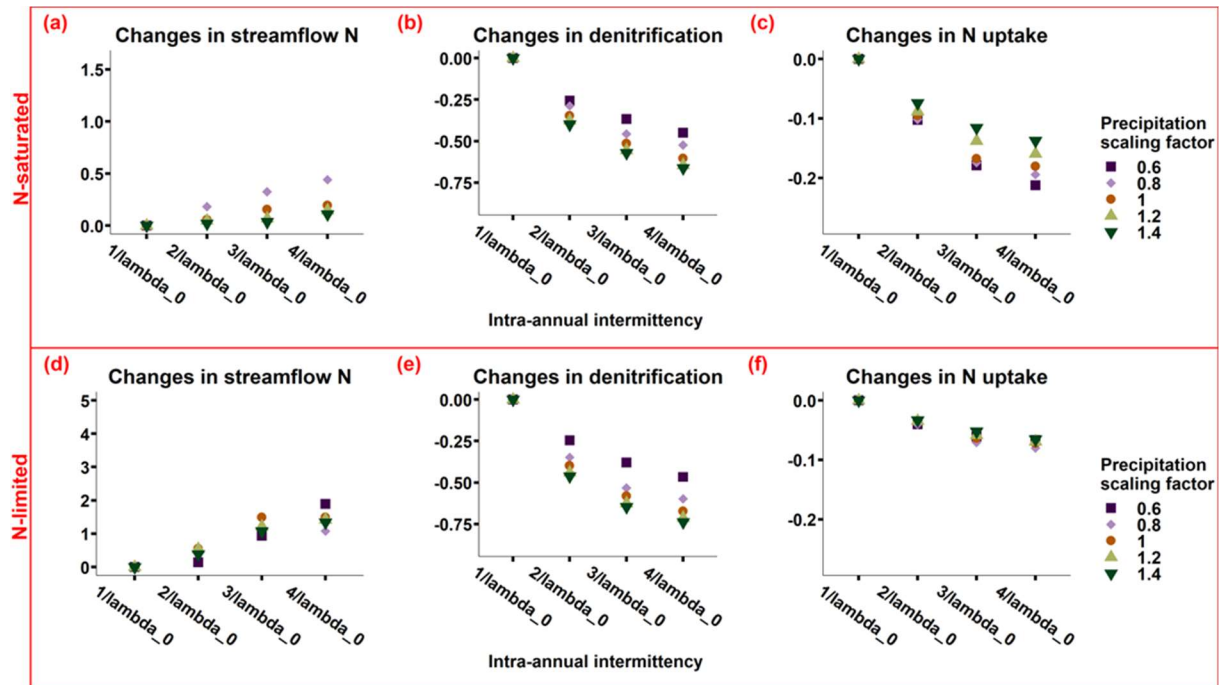
Figure 5. Sensitivity of cumulative N fluxes over 60 years to intra-annual precipitation intermittency for N-saturated and N-limited scenarios (normalized differences relative to baseline (1/λ_0). The x-axis is intermittency, the y-axis is normalized change of other intermittencies relative to their baseline intermittency scenarios (1/λ_0) for every precipitation scaling factor (different precipitation scaling factor scenarios have different baseline intermittency scenarios). The top panels are N-saturated and bottom panels are N-limited scenarios.

3.2.2 The effects of interannual precipitation intermittency on N export.

Greater interannual intermittency and higher levels of precipitation increased streamflow N export and this effect was consistent across both N-limited and N-saturated scenarios (Figure 6). Denitrification exhibited two distinct responses to interannual intermittency. First, when the intermittency exceeded $2/\lambda\_0$, there was a significant increase in denitrification, which occurred because higher interannual intermittency corresponded with more precipitation per rainfall event, resulting in higher soil moisture levels across the landscape and triggering denitrification in non-hotspot patches (Figure 6b, e). However, denitrification started decreasing once interannual intermittency was larger than $3/\lambda\_0$. At the highest interannual intermittency levels, increasing the duration of dry months decreased denitrification to a greater extent than larger storms

467   increased it. Plant uptake generally decreased with higher levels of interannual intermittency,

468   which occurred because long-term drought slowed plant growth (Figure S4b). It is worth noting

469   that the magnitude of streamflow N and denitrification in interannual intermittency scenarios is

470   much larger than that of the scenarios for intra-annual intermittency (Figure 4 and Figure 6).


471
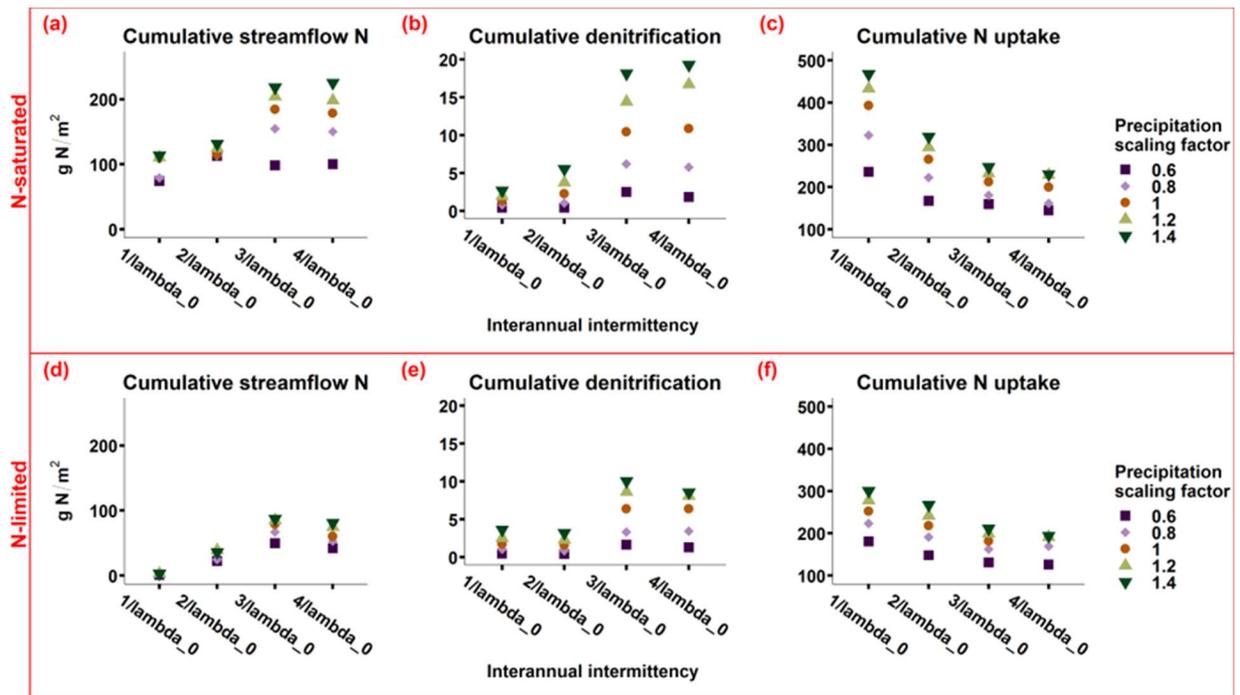
Figure 6. Sensitivity of cumulative N fluxes over 60 years (absolute value) to interannual
precipitation intermittency for N-saturated and N-limited scenarios. The x-axis is the duration of
dry days between rainfall events. Interannual intermittency increases from left to right.

475   Denitrification and plant N uptake were slightly more sensitive to interannual

476   intermittency in N-saturated scenarios than in N-limited scenarios (Figure 7). This occurred

477   because changes in denitrification and plant growth were constrained by N availability in N-

478   limited scenarios and therefore less responsive to precipitation changes. Streamflow N export

479   was more sensitive to interannual intermittency in N-limited scenarios compared to N-saturated

480   scenarios (Figure 7a, d). In N-limited scenarios, drier scenarios showed greater changes to

481   interannual intermittency than wetter scenarios, while in N-saturated scenarios wetter scenarios

482   showed greater changes. This occurred because in N-limited scenarios, drier scenarios had less

483   denitrification and plant uptake, resulting in more N available to be flushed to the stream. It

484   worth noting that in the N-limited scenario, interannual precipitation intermittency caused the

485   largest changes in streamflow N export compared to intra-annual intermittency and interannual

486   variability.
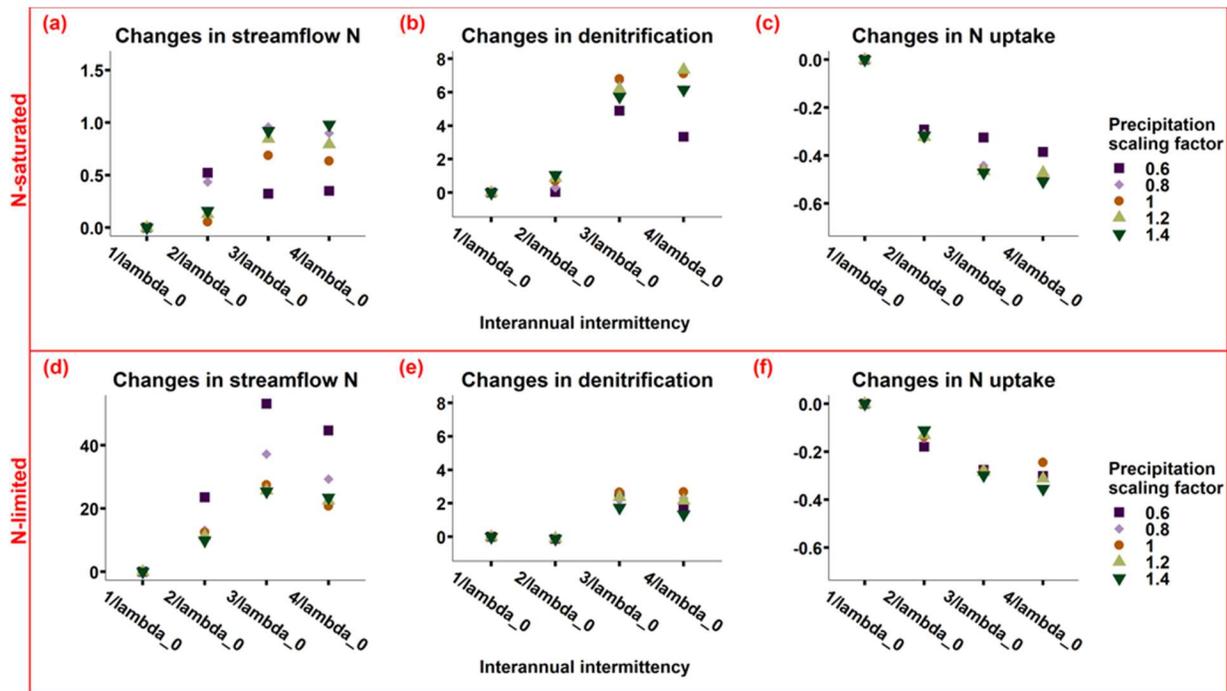
487

488   *Figure 7. Sensitivity of cumulative N fluxes over 60 years to interannual precipitation*
489   *intermittency for N-saturated and N-limited scenarios (differences are relative to baseline*
490   *intermittency; $1/\lambda\_0$). The x-axis is intermittency, the y-axis is normalized change of other*
491   *intermittencies relative to their baseline intermittency scenarios ($1/\lambda\_0$) for every precipitation*
492   *scaling factor. The top panels are N limited and the bottom panels are N saturated scenarios.*
493   *Note that the scale of y-axis for changes in streamflow N is different for N-saturated and N-*
494   *limited scenarios.*

495   3.2.3 The effect of interannual precipitation variability on N export

496   In general, scenarios with higher precipitation variance and wetter scaling factors resulted

497   in more streamflow N export (Figure 8). However, for wetter future scenarios, a precipitation

498   scaling factor of 1.2 (rather than 1.4) resulted in the highest streamflow N export (Figure 8a, d).

499 This suggests there is a threshold of precipitation increase above which higher flushing capacity

500 is compensated by less available N for flushing with higher denitrification and plant uptake. This

501 can occur because more precipitation can cause higher denitrification and plant N uptake, which

502 can reduce the amount of N available for flushing. Moreover, denitrification rates increased with

503 higher precipitation variance and a higher precipitation scaling factor (Figure 8b, e). Notably,

504 both streamflow N export and denitrification rates were higher in N-saturated compared to N-

505 limited scenarios, due to greater nitrate inputs in N-saturated scenarios.
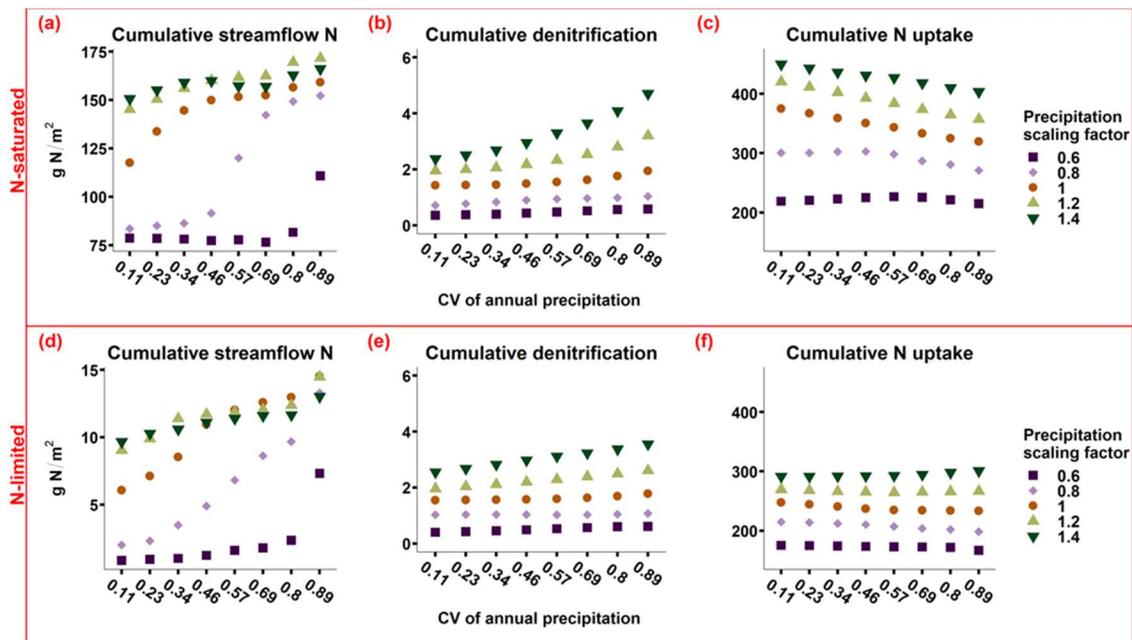
506

507 Figure 8. Cumulative N fluxes over 60 years (absolute value) relative to interannual
508 precipitation variability and scaling factors for N-limited and N-saturated scenarios. The x axis
509 is the coefficient of variation for annual precipitation, the y axis is the cumulative N fluxes over
510 60 years.

511   The sensitivity of N fluxes to precipitation variability differed between N-limited and N-

512 saturated scenarios and was also affected by the precipitation scaling factors (i.e., drier vs. wetter

513 futures; Figure 9). Streamflow N export was more sensitive to precipitation variability in N-

514 limited than in N-saturated scenarios, particularly for the drier future scenarios (Figure 9a, d),

26

515   while denitrification showed the opposite trend (Figure 9b, e). The magnitude of sensitivity for

516   plant N uptake was similar between N-limited and N-saturated scenarios, but the direction of

517   effects (i.e., increases or decreases) differed and was affected by the precipitation scaling factor.

518   In the N-limited scenarios, plant N uptake decreased with precipitation variability in drier future

519   scenarios but increased in wetter future scenarios, suggesting that higher precipitation variability

520   can increase plant growth when there is more water available, even if the watershed is N-limited.

521   On the other hand, higher precipitation variability and water stress will suppress plant growth. In

522   N-saturated scenarios, plant N uptake generally decreased with higher precipitation variability,

523   except in some drier scenarios with smaller variability. This suggests that in N-saturated

524   watersheds, less precipitation combined with moderately higher variability can promote plant

525   growth to some extent.
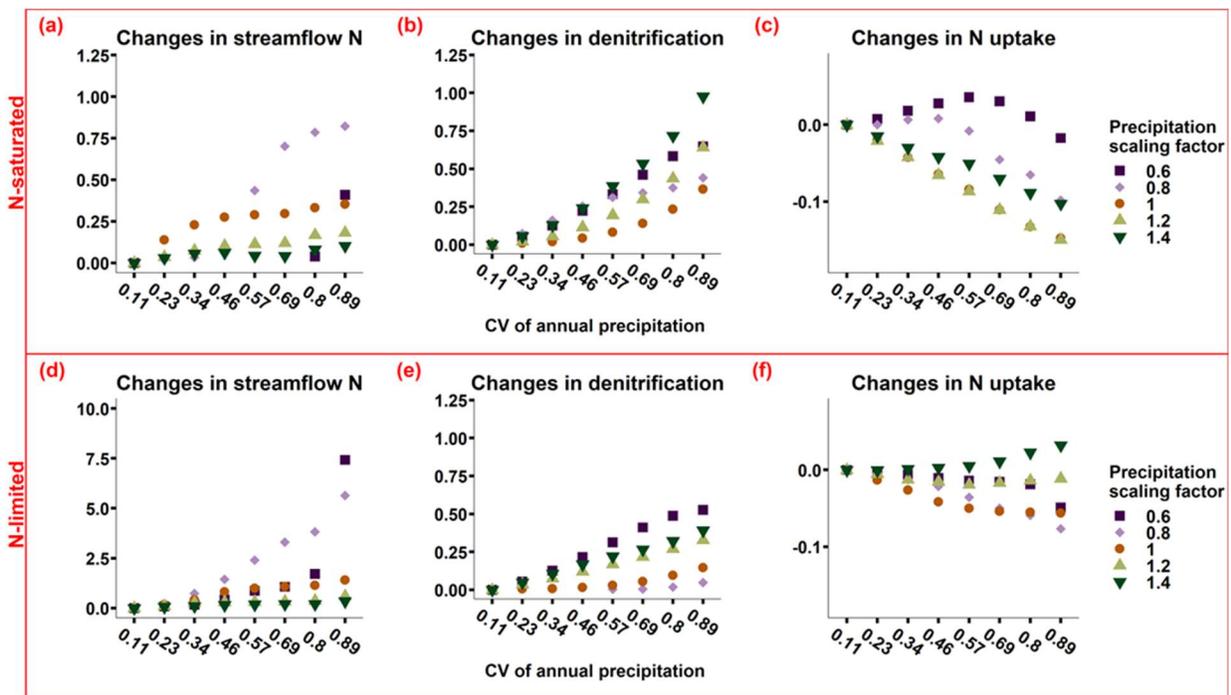
526

527   *Figure 9. Sensitivity of cumulative N fluxes over 60 years to interannual precipitation variability*
528   *for N-saturated and N-limited scenarios (differences are relative to the baseline variability*
529   *scenario which is 0.11). The x axis is the coefficient of variation for annual precipitation. The y*

4 Discussion

Over the last century, atmospheric N deposition and climate change have increased both greenhouse gas emissions (e.g., NO and nitrous oxide; N_2O) and stream nitrate export from many dryland watersheds in western North America (Groffman, 2012; Homyak et al., 2016; Krichels et al., 2022). Because these gaseous and hydrologic N fluxes can exacerbate global climate change, decrease aquatic biodiversity, and harm human health (Galloway et al., 2003; Gustine et al., 2022; Meyer et al., 2022), it is important to be able to predict how they will change in the future. In drylands, N export is highly sensitive to both N deposition rates and precipitation variability (Welter et al., 2005; Ye & Grimm, 2013); interannual precipitation variability and intermittency are both projected to increase in drylands under future climate change (Pörtner et al., 2022). However, our ability to model and predict future N export remains limited, particularly in response to these interacting drivers.

Previous research has mainly focused on how the amount of precipitation in storm events can affect ecosystem function (e.g., Jarvis et al., 2007; Kennedy et al., 2021; Stephens et al., 2020; Ye & Grimm, 2013); fewer studies have also explored the cumulative effects of precipitation variability across multiple decades (D'Odorico et al., 2003; Gherardi & Sala, 2015; Jiang et al., 2019; Porporato et al., 2003). Further research is needed to examine how different types of precipitation intensification (e.g., increasing intermittency vs. variability) will influence biogeochemical cycling, and to investigate how these effects can differ between N-limited and N-saturated watersheds. In this study, we conducted a modeling analysis to understand how N saturation status, precipitation intermittency, variability, and the total amount of precipitation can

555   interact to influence N export in a dryland watershed in California. We found that streamflow N

556   was more sensitive to intensification of the precipitation regime in N-limited than N-limited

557   scenarios, whereas the opposite was true for denitrification. Furthermore, changes in interannual

558   precipitation intermittency had the largest effect on streamflow N and denitrification, suggesting

559   that N export may become an even greater threat to water quality when prolonged drought is

560   followed by more intense storm events.

561   **4.1 Identifying N deposition thresholds for capacity saturation**

562   To distinguish between kinetic (i.e., seasonal) and capacity (i.e., long-term) N saturation

563   (Lovett & Goodale 2011), we developed a simulation modeling approach that quantifies

564   watershed responses to N deposition under different rainfall seasonality regimes. By identifying

565   the amount of N deposition required for precipitation regimes to no longer modify N export, we

566   can approximate when N deposition has truly exceeded the capacity for plants and microbes to

567   take it up. This approach assumes that kinetic N saturation is more sensitive to precipitation

568   seasonality and timing, which affects plant and microbial N assimilation, while capacity N

569   saturation is less sensitive.

570   We found that the Bell 4 watershed can become capacity saturated when N deposition

571   reaches 2 g m^{-2} year^{-1} over about 40 years (Figure 3). This suggests that the watershed—which

572   has a current mean N deposition rate greater than 2 g m^{-2} year^{-1}—has already approached

573   capacity saturation. It is important to note that the threshold we identified is location-specific and

574   is likely to vary with the size, vegetation cover, and climate of a given watershed (Dijkstra et al.,

575   2004; Yu et al., 2018). On average, N deposition is around 0.7 g m^{-2} year^{-1} in dryland watersheds

576   globally and rates are expected to double by 2050 (Benish et al., 2022; Galloway et al., 2008;

577   Kanakidou et al., 2016). Given these increases, many other dryland watersheds could begin to

578   exceed the N deposition thresholds required to shift from a kinetic to capacity saturation in the

579   coming decades. These shifts can pose a major threat to water quality, aquatic ecosystems, and

580   human health. Our study provides a useful modeling approach that can be applied to other

581   watersheds to determine N deposition thresholds for establishing capacity N saturation.

582   **4.2 The role of N saturation status**

583   Does an increase in N deposition lead to greater N export or N uptake? It is essential to

584   distinguish between N-saturated and N-limited watersheds to unravel how changes in the total

585   amount of precipitation and its intermittency or variability will influence watershed processes

586   (Rudgers et al., 2023). In our model setup, N deposition was 100 times higher in N-saturated

587   than in N-limited scenarios. However, the N-saturated/N-limited ratios for various N fluxes (i.e.,

588   streamflow N, denitrification, N uptake) were all smaller than 100 and varied among scenarios

589   (Figure S5). This suggests that N partitioning and soil N storage also changed in response to N-

590   deposition. Not surprisingly, streamflow N had the highest N-saturated/N-limited ratios, ranging

591   from 15 to 80. Denitrification and N uptake, on the other hand, only experienced modest 1-2-fold

592   increases in response to N saturation (Figure S5). Because most atmospherically deposited N is

593   exported to streams, projected decreases in streamflow (Ficklin et al., 2022; Stephens et al.,

594   2020) could lead to even higher streamflow nitrate concentrations, particularly under increased

595   interannual precipitation variability (Gallo et al., 2015; Ye & Grimm, 2013).

596   As precipitation regimes become more intermittent and/or variable, N-limited watersheds

597   can retain less N in soil (Winter et al., 2023) and N saturated watershed can become more

598   saturated or retain more N in soil . In N-limited scenarios, total N export was 25 times higher

599   than the rate of atmospheric N deposition over the 60-year simulation period. This occurred in

600   large part due to declines in plant productivity and N uptake. In N-saturated scenarios, on the

601   other hand, the ratio between N inputs and outputs was consistently less than one, with

602   approximately 20% to 60% of the atmospheric N deposition being exported over the 60-year

603   simulation period (Figure 10). The highest N export transfer efficiencies (calculated as the ratio

604   between total N export and N deposition) occurred with high interannual intermittency, while

605   high intra-annual intermittency produced the lowest. Additionally, transfer efficiency can

606   become even higher in a wetter future due to increases in streamflow. Thus, in N-limited

607   scenarios (particularly in a wetter future), increases in precipitation interannual intermittency can

608   increase N export efficiency, thereby reducing N retention capacity in soil. However, our result

609   should be interpreted with care since 25 times higher N transfer efficiency will eventually

610   deplete the N in soil. Conversely, in N-saturated scenarios, a drier future will have lower transfer

611   efficiencies, which can intensify N saturation. This is corroborated by a recent meta-analysis

612   globally, which found that reduced precipitation can increase soil N storage over long-term

613   studies, particularly precipitation decreases by more than 25% (Wu et al., 2022).


614
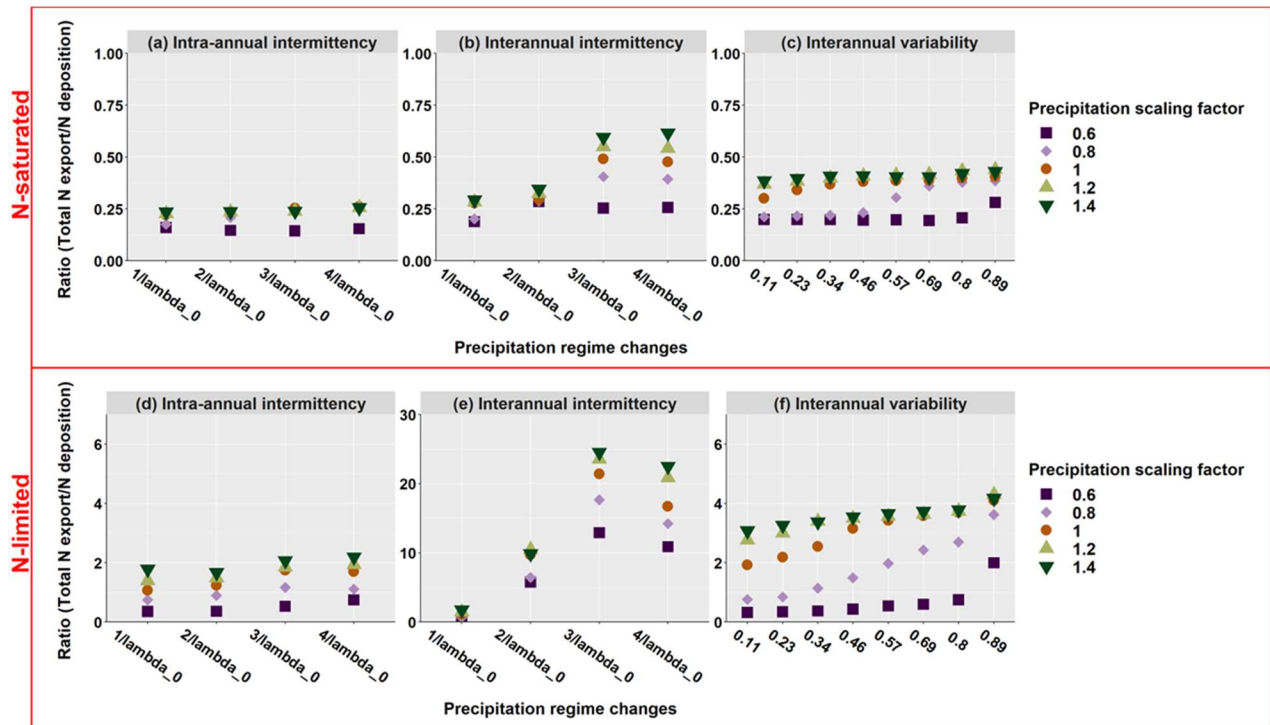
Figure 10. The ratio of total N export (streamflow N and denitrification) to N deposition and its response to precipitation regime changes. For N-saturated scenarios, the N deposition rate was 5 g m^{-2} year^{-1}, for N-limited scenarios, it was 0.05 g m^{-2} year^{-1}. Ratios larger than 1 indicates N outputs are larger than N inputs and vice versa.

4.3 The role of changing precipitation regimes

Recent studies have found that precipitation amount and variability both play an important role in driving ecosystem responses to climate change (Gherardi & Sala, 2015, 2019; Jiang et al., 2019; Rudgers et al., 2023). Here we extend those studies to also examine the role of precipitation intermittency and focus on how it affects streamflow N export. In our experimental setup, we ensured water balance among all scenarios (e.g., scenarios with high vs. low interannual intermittency at a given amount of total precipitation had the same total rainfall over the 60-year simulation period). Thus, longer droughts were followed by more precipitation after drought. Thus interannual intermittency scenarios varied both the timing of storms and their magnitude, whereas interannual precipitation variability scenarios only varied the relative magnitude of storms (e.g., some become larger and some become smaller with increasing variability; Figure 1c). We found that increases in interannual intermittency produced the largest increases (with the greatest variance) in streamflow N among precipitation regime scenarios (Figure 11a). Conversely, interannual variability had the smallest effect on streamflow N. These findings suggest that prolonged drought followed by larger, more intense storms can have the strongest effect on streamflow N. This occurs because multi-year droughts that occur with greater intermittency can reduce N uptake by plants and enable N to accumulate in soils (Krichels et al., 2022; Winter et al., 2023). Subsequent storms then flush accumulated N to streams before plants can take it up.

Denitrification exhibited the most substantial increases with increasing interannual intermittency, whereas it slightly decreased with increasing intra-annual intermittency (Figure

640   11b). This pattern arose because denitrification is strongly influenced by soil moisture and

641   therefore the amount of precipitation in storm events (Homyak et al., 2016). Increases in both

642   interannual intermittency and variability had large effects on the size of individual storms, while

643   increases in intra-annual intermittency had relatively smaller effects.

644   Higher precipitation intra-annual and interannual intermittency and variability can both

645   reduce plant growth and corresponding N uptake, but increases in interannual intermittency,

646   which lead to fewer, more intense storms, exert a stronger influence than changes in variability

647   alone (which only affects the relative size of storms without changing their timing). These

648   findings have important implications for designing field and laboratory experiments aimed at

649   understanding plant responses to changing precipitation regimes. Such experiments should not

650   only consider the important roles of storm size and variance (as identified by Gherardi & Sala

651   (2015) and Rudgers et al. (2023)), but should also incorporate intermittency as a key driver.

652
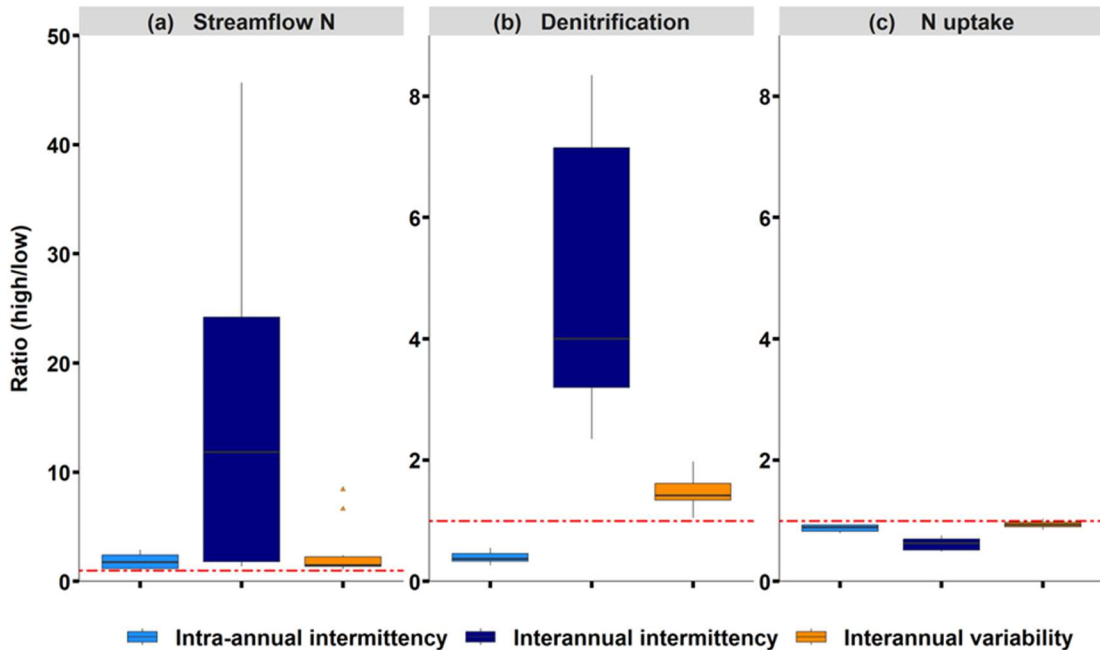
Figure 11. The distribution of ratios of highest intermittency/variability to lowest for different N fluxes. For intermittency this is the ratio between 4/lambda_0 and 1/lambda_0, for variability this is the ratio between 0.89 CV and 0.11 CV. The distribution consists of outputs from all N saturation and precipitation scaling factor scenarios and the variance of distribution indicates how sensitive these N fluxes were to intra-annual intermittency, interannual intermittency, and interannual variability. Note that the y-axis for panel a is on a different scale than for panels b and c. The red dashed line represents a ratio of 1, above which N fluxes increases with intensified precipitation regime and below 1 indicates a decrease.

4.4 The role of total precipitation amount in N-limited systems

Does more total precipitation result in higher N export? When transitioning from drier to wetter future scenarios, denitrification was the most affected, followed by streamflow N, while plant N uptake was least affected (Figure 12 d, e, and f). With a 2.3 fold increase of precipitation (from a 0.6 to a 1.4 scaling factor), median denitrification increased approximately 5 to 7 fold, and this response was slightly greater in N saturated scenarios compared to N-limited scenarios (Figure 12e). This finding aligns with the fact that denitrification is strongly influenced by soil moisture and available nitrate (Poblador et al., 2017). Denitrification is also strongly influenced by soil C (represented as a function of soil respiration in RHESSys), which was higher in wetter

670   future and N-saturated scenarios. Conversely, streamflow N in N-limited scenarios was more

671   responsive to changes in the precipitation scaling factor than in N-saturated scenarios (Figure

672   12d). In N-limited scenarios, streamflow N increased the precipitation scaling factor, reaching

673   approximately 3.5 times higher than baseline in scenarios with a scaling factor of 1.2. However,

674   it reached an asymptote once the scaling factor exceeded 1.2. This suggests that, for N-limited

675   scenarios, increases in total precipitation do not necessarily translate into higher streamflow N

676   because additional water can enhance denitrification, plant N uptake, and reduce nitrification.

677   Because the effects of total precipitation on streamflow N export are non-linear, it can be

678   challenging to predict N export as precipitation regimes continue to change, particularly in N-

679   limited watersheds (Harms & Grimm, 2008; Homyak et al., 2016).

680   Changes in the amount of precipitation can also interact with N saturation status to

681   modify various N fluxes. For example, a higher precipitation scaling factor enhanced the N

682   saturation effect on denitrification and its variability (Figure 12h). Alternatively, in drier future

683   scenarios the ratio between N-saturated to N-limited denitrification was smaller than 1 (Figure

684   12h), suggesting that a drier future can largely inhibit (or even reverse) the N saturation effect,

685   even with 100 times higher N deposition (Wu et al., 2022). With respect to streamflow N, a

686   higher precipitation scaling factor reduced the effects of N saturation and its variability (Figure

687   12g). This aligns with predictions that a drier future would lead to greater N export to streams

688   and a lower flux to the atmosphere through denitrification (Cregger et al., 2014). Our findings

689   also corroborate recent studies showing that interactions between N deposition and the total

690   amount of precipitation drive N export in drylands (Li et al., 2022).

691   Although increases or decreases in the total amount of precipitation had smaller effects

692   on N fluxes than increases in intermittency and/or variability, they interacted with precipitation

693   timing to amplify or attenuate their effects. In N-limited scenarios, streamflow N export

694   increased with higher intermittency and variability, but a drier future exaggerated this response

695   whereas a wetter future dampened it (e.g., Figure 5d, Figure 7d, and Figure 9d). Although a

696   wetter future may lead to greater overall streamflow N export (e.g., Figure 8d), a drier future can

697   result in more substantial increases in streamflow N export (Figure 9d). Furthermore, even minor

698   decreases in the precipitation scaling factor could substantially increase streamflow N (e.g.,

699   Figure 9d and Figure 12g; 0.8 and 0.6 precipitation scaling factors). Thus, the total amount of

700   precipitation can play a critical threshold role in driving how N fluxes respond to increases in

701   precipitation variability and timing (Ficklin et al., 2022).
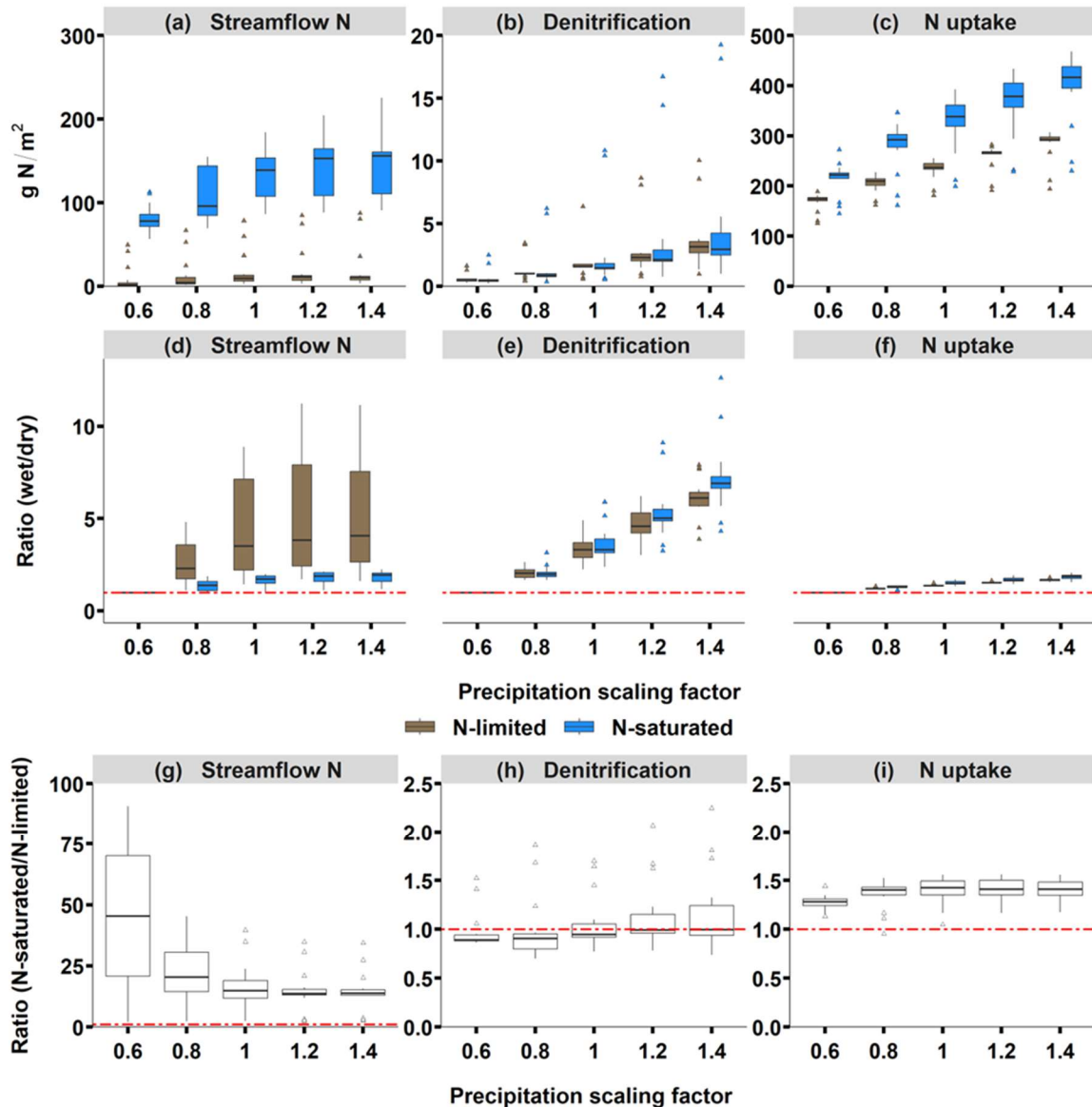
Figure 12. The effect of drier or wetter conditions on N fluxes. The top panels a, b, and c represent how cumulative N fluxes over 60 years change with precipitation scaling factor. Each distribution contains both N saturation statuses and all precipitation regime changes. The middle panels of d, e, and f represent the ratio of fluxes between precipitation scaling factors larger than 0.6 and the driest scaling factor (i.e., 0.6). The bottom panels g, h and i represent the ratio of fluxes in N-saturated and N-limited conditions and how they vary with the precipitation scaling factor. The dashed blue line denotes a ratio equal to 1.

4.5 Study implications

Predicting future N export in drylands requires considering interaction between hotspots (defined as wetter microsites in the soil that have disproportionately high rates of

713 biogeochemical cycling) and hot moments (defined as wet periods after a prolonged dry spell)

714 rather than treating them as separate entities (Groffman et al., 2009; Kuzyakov & Blagodatskaya,

715 2015; Pinay et al., 2015). Our study revealed that the interannual intermittency exhibited the

716 largest influence on streamflow N and denitrification. Interannual intermittency scenarios

717 incorporated increases in both the timing and magnitude of storms (with the same total

718 precipitation over the simulation period for a given precipitation multiplier). Following

719 prolonged drought, large storms can be viewed as hot moments. Once the amount of

720 precipitation during these hot moments surpassed a certain threshold (e.g., $2/\lambda$ in Figure 7e),

721 denitrification was activated in patches across the basin that were not designated as microscale

722 hotspots. This generated a more dynamic distribution of "hotspots" due to the timing of hot

723 moments. To better account for the interdependence between hotspots and hot moments,

724 Bernhardt et al. (2017) proposed a new term more comprehensive term: "ecosystem control

725 points." This new term incorporates both spatial and temporal dynamics instead of addressing

726 them independently (Bernhardt et al., 2017). Our research in a dryland chaparral watershed

727 illustrates how ecosystem control points drive N export under a range of future scenarios.

728   Our modeling framework considered interactions between N saturation status and several

729 ways that precipitation regimes can change. This framework can serve as a tool for

730 understanding the specific mechanisms driving future N export under climate change. For

731 example, our model framework highlights the importance of considering the role of interannual

732 intermittency (not just variability) when examining how future precipitation will influence N

733 fluxes. This approach can help researcher determine the interannual intermittency thresholds that

734 trigger substantial increases in denitrification, which can in turn help them design precipitation

735 manipulation experiments with appropriate intermittency levels.

5 Conclusion

We developed a comprehensive modeling framework that incorporates the role of both N deposition and intensification of the precipitation regime (i.e., the total amount, intermittency, and variability) in driving N export in dryland ecosystems. We identified a critical N deposition threshold of around 2 g m^{-2} year^{-1} beyond which the watershed shifts from N-limited to N-saturated. Our findings reveal that streamflow N export in N-limited watersheds is more sensitive to changes in the timing of precipitation compared to N-saturated watersheds, whereas denitrification in N-saturated watersheds was more responsive to changes in precipitation timing in N-saturated watersheds. Additionally, we found that a drier future exaggerated the effects of precipitation timing on N export, while there was no uniform response under a wetter future. Notably, among the various precipitation regime changes, interannual intermittency caused the largest changes in N export compared to other characteristics of the precipitation regime. Our modeling framework helps disentangle the key drivers of N fluxes amid complex interactions between N saturation and precipitation in dryland watersheds. We found that interannual rainfall intermittency enables solutes like nitrate to build up in hotspots and then be flushed to streams with subsequent intense storms—thus as rainfall intermittency and associated droughts continue to increase, N export will become an even greater threat to water security.

762 **References**

763 Abatzoglou, J. T. (2013). Development of gridded surface meteorological data for ecological

764   applications and modelling. *International Journal of Climatology*, *33*(1), 121–131.

765   https://doi.org/10.1002/joc.3413

766 Aber, J. D., Nadelhoffer, K. J., Steudler, P., & Melillo, J. M. (1989). Nitrogen Saturation in

767   Northern Forest Ecosystems: Excess nitrogen from fossil fuel combustion may stress the

768   biosphere. *BioScience*, *39*(6), 378–386. https://doi.org/10.2307/1311067

769 Allen, M. R., & Ingram, W. J. (2002). Constraints on future changes in climate and the

770   hydrologic cycle. *Nature*, *419*(6903), 224–232. https://doi.org/10.1038/nature01092

771 Benish, S. E., Bash, J. O., Foley, K. M., Appel, K. W., Hogrefe, C., Gilliam, R., & Pouliot, G.

772   (2022). Long-term regional trends of nitrogen and sulfur deposition in the United States

773   from 2002 to 2017. *Atmospheric Chemistry and Physics*, *22*(19), 12749–12767.

774   https://doi.org/10.5194/acp-22-12749-2022

775 Bernhardt, E. S., Blaszczak, J. R., Ficken, C. D., Fork, M. L., Kaiser, K. E., & Seybold, E. C.

776   (2017). Control Points in Ecosystems: Moving Beyond the Hot Spot Hot Moment

777   Concept. *Ecosystems*, *20*(4), 665–682. https://doi.org/10.1007/s10021-016-0103-y

778 Burke, W. D., Tague, C., Kennedy, M. C., & Moritz, M. A. (2021). Understanding How Fuel

779   Treatments Interact With Climate and Biophysical Setting to Affect Fire, Water, and

780   Forest Health: A Process-Based Modeling Approach. *Frontiers in Forests and Global*

781   *Change*, *3*. https://doi.org/10.3389/ffgc.2020.591162

782   Bytnerowicz, A., & Fenn, M. E. (1996). Nitrogen deposition in California forests: a review.

783   *Environmental Pollution, Vol. 92(2): 127-146*. Retrieved from

784   https://www.fs.usda.gov/research/treesearch/24944

785   Chaney, N. W., Wood, E. F., McBratney, A. B., Hempel, J. W., Nauman, T. W., Brungard, C.

786   W., & Odgers, N. P. (2016). POLARIS: A 30-meter probabilistic soil series map of the

787   contiguous United States. *Geoderma*, *274*, 54–67.

788   https://doi.org/10.1016/j.geoderma.2016.03.025

789   Chen, X., Tague, C. L., Melack, J. M., & Keller, A. A. (2020). Sensitivity of nitrate

790   concentration-discharge patterns to soil nitrate distribution and drainage properties in the

791   vertical dimension. *Hydrological Processes*, *34*(11), 2477–2493.

792   https://doi.org/10.1002/hyp.13742

793   Cregger, M. A., McDowell, N. G., Pangle, R. E., Pockman, W. T., & Classen, A. T. (2014). The

794   impact of precipitation change on nitrogen cycling in a semi-arid ecosystem. *Functional*

795   *Ecology*, *28*(6), 1534–1544. https://doi.org/10.1111/1365-2435.12282

796   Dentener, F., Drevet, J., Lamarque, J. F., Bey, I., Eickhout, B., Fiore, A. M., et al. (2006).

797   Nitrogen and sulfur deposition on regional and global scales: A multimodel evaluation.

798   *Global Biogeochemical Cycles*, *20*(4). https://doi.org/10.1029/2005GB002672

799   Dickinson, R. E., Shaikh, M., Bryant, R., & Graumlich, L. (1998). Interactive Canopies for a

800   Climate Model. *Journal of Climate*, *11*(11), 2823–2836. https://doi.org/10.1175/1520-

801   0442(1998)011<2823:ICFACM>2.0.CO;2

802   Dijkstra, F. A., Hobbie, S. E., Knops, J. M. H., & Reich, P. B. (2004). Nitrogen deposition and

803   plant species interact to influence soil carbon stabilization. *Ecology Letters*, *7*(12), 1192–

804   1198. https://doi.org/10.1111/j.1461-0248.2004.00679.x

805   D'Odorico, P., Laio, F., Porporato, A., & Rodriguez-Iturbe, I. (2003). Hydrologic controls on

806   soil carbon and nitrogen cycles. II. A case study. *Advances in Water Resources*, *26*(1),

807   59–70. https://doi.org/10.1016/S0309-1708(02)00095-7

808   Dunn, P. H., Barro, S. C., Wells, W. G., Poth, M. A., Wohlgemuth, P. M., & Colver, C. G.

809   (1988). *The San Dimas experimental forest: 50 years of research* (No. PSW-GTR-104)

810   (p. PSW-GTR-104). Berkeley, CA: U.S. Department of Agriculture, Forest Service,

811   Pacific Southwest Forest and Range Experiment Station. https://doi.org/10.2737/PSW-

812   GTR-104

813   Eagleson, P. S. (1978). Climate, soil, and vegetation: 3. A simplified model of soil moisture

814   movement in the liquid phase. *Water Resources Research*, *14*(5), 722–730.

815   https://doi.org/10.1029/WR014i005p00722

816   Farquhar, G. D., & von Caemmerer, S. (1982). Modelling of Photosynthetic Response to

817   Environmental Conditions. In O. L. Lange, P. S. Nobel, C. B. Osmond, & H. Ziegler

818   (Eds.), *Physiological Plant Ecology II: Water Relations and Carbon Assimilation* (pp.

819   549–587). Berlin, Heidelberg: Springer. https://doi.org/10.1007/978-3-642-68150-9_17

820   Ficklin, D. L., Null, S. E., Abatzoglou, J. T., Novick, K. A., & Myers, D. T. (2022).

821   Hydrological Intensification Will Increase the Complexity of Water Resource

822   Management. *Earth's Future*, *10*(3), e2021EF002487.

823   https://doi.org/10.1029/2021EF002487

824   Fischer, E. M., Beyerle, U., & Knutti, R. (2013). Robust spatially aggregated projections of

825   climate extremes. *Nature Climate Change*, *3*(12), 1033–1038.

826   https://doi.org/10.1038/nclimate2051

827   Gallo, E. L., Meixner, T., Aoubid, H., Lohse, K. A., & Brooks, P. D. (2015). Combined impact

828   of catchment size, land cover, and precipitation on streamflow and total dissolved

829   nitrogen: A global comparative analysis. *Global Biogeochemical Cycles*, *29*(7), 1109–

830   1121. https://doi.org/10.1002/2015GB005154

831   Galloway, J. N., Aber, J. D., Erisman, J. W., Seitzinger, S. P., Howarth, R. W., Cowling, E. B.,

832   & Cosby, B. J. (2003). The Nitrogen Cascade. *BioScience*, *53*(4), 341–356.

833   https://doi.org/10.1641/0006-3568(2003)053[0341:TNC]2.0.CO;2

834   Galloway, J. N., Townsend, A. R., Erisman, J. W., Bekunda, M., Cai, Z., Freney, J. R., et al.

835   (2008). Transformation of the Nitrogen Cycle: Recent Trends, Questions, and Potential

836   Solutions. *Science*, *320*(5878), 889–892. https://doi.org/10.1126/science.1136674

837   Garcia, E. S., & Tague, C. L. (2015). Subsurface storage capacity influences climate–

838   evapotranspiration interactions in three western United States catchments. *Hydrology and*

839   *Earth System Sciences*, *19*(12), 4845–4858. https://doi.org/10.5194/hess-19-4845-2015

840   Garcia, Elizabeth S., Tague, C. L., & Choate, J. S. (2016). Uncertainty in carbon allocation

841   strategy and ecophysiological parameterization influences on carbon and streamflow

842   estimates for two western US forested watersheds. *Ecological Modelling*, *342*, 19–33.

843   https://doi.org/10.1016/j.ecolmodel.2016.09.021

844   Gherardi, L. A., & Sala, O. E. (2015). Enhanced precipitation variability decreases grass- and

845   increases shrub-productivity. *Proceedings of the National Academy of Sciences*, *112*(41),

846   12735–12740. https://doi.org/10.1073/pnas.1506433112

847   Gherardi, L. A., & Sala, O. E. (2019). Effect of interannual precipitation variability on dryland

848   productivity: A global synthesis. *Global Change Biology*, *25*(1), 269–276.

849   https://doi.org/10.1111/gcb.14480

850   Groffman, P. M. (2012). Terrestrial denitrification: challenges and opportunities. *Ecological*

851   *Processes*, *1*(1), 1–11. https://doi.org/10.1186/2192-1709-1-11

852   Groffman, P. M., Butterbach-bahl, K., Fulweiler, R. W., Gold, A. J., Morse, J. L., Stander, E. K.,

853   et al. (2009). Challenges to incorporating spatially and temporally explicit phenomena

854   (hotspots and hot moments) in denitrification models. *Biogeochemistry*, *93*(1–2), 49–77.

855   https://doi.org/10.1007/s10533-008-9277-5

856   Gustine, R. N., Hanan, E. J., Robichaud, P. R., & Elliot, W. J. (2022). From burned slopes to

857   streams: how wildfire affects nitrogen cycling and retention in forests and fire-prone

858   watersheds. *Biogeochemistry*, *157*(1), 51–68. https://doi.org/10.1007/s10533-021-00861-

859   0

860   Hanan, E. J., Tague, C. (Naomi), & Schimel, J. P. (2017). Nitrogen cycling and export in

861   California chaparral: the role of climate in shaping ecosystem responses to fire.

862   *Ecological Monographs*, *87*(1), 76–90. https://doi.org/10.1002/ecm.1234

863   Hanan, E. J., Tague, C., Choate, J., Liu, M., Kolden, C., & Adam, J. (2018). Accounting for

864   disturbance history in models: using remote sensing to constrain carbon and nitrogen pool

865   spin-up. *Ecological Applications: A Publication of the Ecological Society of America*,

866   *28*(5), 1197–1214. https://doi.org/10.1002/eap.1718

867   Hanan, E. J., Ren, J., Tague, C. L., Kolden, C. A., Abatzoglou, J. T., Bart, R. R., et al. (2021).

868   How climate change and fire exclusion drive wildfire regimes at actionable scales.

869   *Environmental Research Letters*, *16*(2), 024051. https://doi.org/10.1088/1748-

870   9326/abd78e

871 Harms, T. K., & Grimm, N. B. (2008). Hot spots and hot moments of carbon and nitrogen

872   dynamics in a semiarid riparian zone. *Journal of Geophysical Research: Biogeosciences*,

873   *113*(G1). https://doi.org/10.1029/2007JG000588

874 Homyak, P. M., Sickman, J. O., Miller, A. E., Melack, J. M., Meixner, T., & Schimel, J. P.

875   (2014). Assessing Nitrogen-Saturation in a Seasonally Dry Chaparral Watershed:

876   Limitations of Traditional Indicators of N-Saturation. *Ecosystems*, *17*(7), 1286–1305.

877   https://doi.org/10.1007/s10021-014-9792-2

878 Homyak, P. M., Blankinship, J. C., Marchus, K., Lucero, D. M., Sickman, J. O., & Schimel, J. P.

879   (2016). Aridity and plant uptake interact to make dryland soils hotspots for nitric oxide

880   (NO) emissions. *Proceedings of the National Academy of Sciences*, *113*(19), E2608–

881   E2616. https://doi.org/10.1073/pnas.1520496113

882 Homyak, P. M., Allison, S. D., Huxman, T. E., Goulden, M. L., & Treseder, K. K. (2017).

883   Effects of Drought Manipulation on Soil Nitrogen Cycling: A Meta-Analysis. *Journal of*

884   *Geophysical Research: Biogeosciences*, *122*(12), 3260–3272.

885   https://doi.org/10.1002/2017JG004146

886 Howarth, R. W., Swaney, D. P., Boyer, E. W., Marino, R., Jaworski, N., & Goodale, C. (2006).

887   The influence of climate on average nitrogen export from large watersheds in the

888   Northeastern United States. *Biogeochemistry*, *79*(1), 163–186.

889   https://doi.org/10.1007/s10533-006-9010-1

890 Hubbert, K. R., Preisler, H. K., Wohlgemuth, P. M., Graham, R. C., & Narog, M. G. (2006).

891   Prescribed burning effects on soil physical properties and soil water repellency in a steep

892   chaparral watershed, southern California, USA. *Geoderma*, *130*(3), 284–298.

893   https://doi.org/10.1016/j.geoderma.2005.02.001

894 Jarvis, P., Rey, A., Petsikos, C., Wingate, L., Rayment, M., Pereira, J., et al. (2007). Drying and

895   wetting of Mediterranean soils stimulates decomposition and carbon dioxide emission:

896   the "Birch effect." *Tree Physiology*, *27*(7), 929–940.

897   https://doi.org/10.1093/treephys/27.7.929

898 Jiang, P., Liu, H., Piao, S., Ciais, P., Wu, X., Yin, Y., & Wang, H. (2019). Enhanced growth

899   after extreme wetness compensates for post-drought carbon loss in dry forests. *Nature*

900   *Communications*, *10*(1), 195. https://doi.org/10.1038/s41467-018-08229-z

901 Kanakidou, M., Myriokefalitakis, S., Daskalakis, N., Fanourgakis, G., Nenes, A., Baker, A. R., et

902   al. (2016). Past, Present and Future Atmospheric Nitrogen Deposition. *Journal of the*

903   *Atmospheric Sciences*, *73*(5), 2039–2047. https://doi.org/10.1175/JAS-D-15-0278.1

904 Kennedy, M. C., Bart, R. R., Tague, C. L., & Choate, J. S. (2021). Does hot and dry equal more

905   wildfire? Contrasting short- and long-term climate effects on fire in the Sierra Nevada,

906   CA. *Ecosphere*, *12*(7), e03657. https://doi.org/10.1002/ecs2.3657

907 Knapp, A. K., Fay, P. A., Blair, J. M., Collins, S. L., Smith, M. D., Carlisle, J. D., et al. (2002).

908   Rainfall Variability, Carbon Cycling, and Plant Species Diversity in a Mesic Grassland.

909   *Science*, *298*(5601), 2202–2205.

910 Knapp, A. K., Hoover, D. L., Wilcox, K. R., Avolio, M. L., Koerner, S. E., La Pierre, K. J., et al.

911   (2015). Characterizing differences in precipitation regimes of extreme wet and dry years:

912   implications for climate change experiments. *Global Change Biology*, *21*(7), 2624–2633.

913   https://doi.org/10.1111/gcb.12888

914   Krichels, A. H., Greene, A. C., Jenerette, G. D., Spasojevic, M. J., Glassman, S. I., & Homyak,

915   P. M. (2022). Precipitation legacies amplify ecosystem nitrogen losses from nitric oxide

916   emissions in a Pinyon–Juniper dryland. *Ecology*, *104*(2), e3930.

917   https://doi.org/10.1002/ecy.3930

918   Kuzyakov, Y., & Blagodatskaya, E. (2015). Microbial hotspots and hot moments in soil:

919   Concept & review. *Soil Biology and Biochemistry*, *83*, 184–199.

920   https://doi.org/10.1016/j.soilbio.2015.01.025

921   Li, Z., Tang, Z., Song, Z., Chen, W., Tian, D., Tang, S., et al. (2022). Variations and controlling

922   factors of soil denitrification rate. *Global Change Biology*, *28*(6), 2133–2145.

923   https://doi.org/10.1111/gcb.16066

924   Lin, L., Webster, J. R., Hwang, T., & Band, L. E. (2015). Effects of lateral nitrate flux and

925   instream processes on dissolved inorganic nitrogen export in a forested catchment: A

926   model sensitivity analysis. *Water Resources Research*, *51*(4), 2680–2695.

927   https://doi.org/10.1002/2014WR015962

928   Lovett, G. M., & Goodale, C. L. (2011). A New Conceptual Model of Nitrogen Saturation Based

929   on Experimental Nitrogen Addition to an Oak Forest. *Ecosystems*, *14*(4), 615–631.

930   https://doi.org/10.1007/s10021-011-9432-z

931   Maxwell, A. E., Warner, T. A., Vanderbilt, B. C., & Ramezan, C. A. (2017). Land Cover

932   Classification and Feature Extraction from National Agriculture Imagery Program

933   (NAIP) Orthoimagery: A Review. *Photogrammetric Engineering & Remote Sensing*,

934   *83*(11), 737–747. https://doi.org/10.14358/PERS.83.10.737

935   Meyer, M. F., Ozersky, T., Woo, K. H., Shchapov, K., Galloway, A. W. E., Schram, J. B., et al.

936   (2022). Effects of spatially heterogeneous lakeside development on nearshore biotic

937   communities in a large, deep, oligotrophic lake. *Limnology and Oceanography*, *67*(12),

938   2649–2664. https://doi.org/10.1002/lno.12228

939   Nash, J. E., & Sutcliffe, J. V. (1970). River flow forecasting through conceptual models part I —

940   A discussion of principles. *Journal of Hydrology*, *10*(3), 282–290.

941   https://doi.org/10.1016/0022-1694(70)90255-6

942   Parker, S. S., & Schimel, J. P. (2011). Soil nitrogen availability and transformations differ

943   between the summer and the growing season in a California grassland. *Applied Soil*

944   *Ecology*, *48*(2), 185–192. https://doi.org/10.1016/j.apsoil.2011.03.007

945   Parton, W. J. (1996). The CENTURY model. In D. S. Powlson, P. Smith, & J. U. Smith (Eds.),

946   *Evaluation of Soil Organic Matter Models* (Vol. 38, pp. 283–291). Springer, Berlin,

947   Heidelberg: Evaluation of Soil Organic Matter Models.

948   Pinay, G., Peiffer, S., De Dreuzy, J.-R., Krause, S., Hannah, D. M., Fleckenstein, J. H., et al.

949   (2015). Upscaling Nitrogen Removal Capacity from Local Hotspots to Low Stream

950   Orders' Drainage Basins. *Ecosystems*, *18*(6), 1101–1120. https://doi.org/10.1007/s10021-

951   015-9878-5

952   Poblador, S., Lupon, A., Sabaté, S., & Sabater, F. (2017). Soil water content drives

953   spatiotemporal patterns of CO_2 and N_2O emissions from a Mediterranean riparian forest

954   soil. *Biogeosciences*, *14*(18), 4195–4208. https://doi.org/10.5194/bg-14-4195-2017

955   Porporato, A., D'Odorico, P., Laio, F., & Rodriguez-Iturbe, I. (2003). Hydrologic Controls on

956   Soil Carbon and Nitrogen Cycles. I. Modeling Scheme. *Advances in Water Resources*,

957   *26*, 45–58. https://doi.org/10.1016/S0309-1708(02)00094-5

958   Pörtner, H.-O., Roberts, D. C., Tignor, M. M. B., Poloczanska, E. S., Mintenbeck, K., Alegría,

959   A., et al. (Eds.). (2022). *Climate Change 2022: Impacts, Adaptation and Vulnerability.*

960   *Contribution of Working Group II to the Sixth Assessment Report of the*

961   *Intergovernmental Panel on Climate Change.*

962   Ren, J., Adam, J. C., Hicke, J. A., Hanan, E. J., Tague, C. L., Liu, M., et al. (2021). How does

963   water yield respond to mountain pine beetle infestation in a semiarid forest? *Hydrology*

964   *and Earth System Sciences*, *25*(9), 4681–4699. https://doi.org/10.5194/hess-25-4681-

965   2021

966   Ren, J., Hanan, E. J., Abatzoglou, J. T., Kolden, C. A., Tague, C. (Naomi) L., Kennedy, M. C., et

967   al. (2022). Projecting Future Fire Regimes in a Semiarid Watershed of the Inland

968   Northwestern United States: Interactions Among Climate Change, Vegetation

969   Productivity, and Fuel Dynamics. *Earth's Future*, *10*(3), e2021EF002518.

970   https://doi.org/10.1029/2021EF002518

971   Ren, J., Hanan, E., Greene, A. C., Tague, C., Krichels, A., Burk, W., et al. (2023). *Simulating the*

972   *role of biogeochemical hotspots in driving nitrogen export from dryland watersheds*

973   (preprint). Preprints. https://doi.org/10.22541/essoar.169168922.25673935/v1

974   Reyes, J. J., Tague, C. L., Evans, R. D., & Adam, J. C. (2017). Assessing the Impact of

975   Parameter Uncertainty on Modeling Grass Biomass Using a Hybrid Carbon Allocation

976   Strategy: A HYBRID CARBON ALLOCATION STRATEGY. *Journal of Advances in*

977   *Modeling Earth Systems*, *9*(8), 2968–2992. https://doi.org/10.1002/2017MS001022

978   Rodriguez-Iturbe, I., Porporato, A., Ridolfi, L., Isham, V., & Coxi, D. R. (1999). Probabilistic

979   modelling of water balance at a point: the role of climate, soil and vegetation.

980   *Proceedings of the Royal Society of London. Series A: Mathematical, Physical and*

981   *Engineering Sciences*, *455*(1990), 3789–3805. https://doi.org/10.1098/rspa.1999.0477

982   Rudgers, J. A., Luketich, A., Bacigalupa, M., Baur, L. E., Collins, S. L., Hall, K. M., et al.

983   (2023). Infrastructure to factorially manipulate the mean and variance of precipitation in

984   the field. *Ecosphere*, *14*(7), e4603. https://doi.org/10.1002/ecs2.4603

985   Ryan, M. G. (1991). Effects of Climate Change on Plant Respiration. *Ecological Applications*,

986   *1*(2), 157–167. https://doi.org/10.2307/1941808

987   Ryan, T. M. (1991). *Soil Survey of Angeles National Forest Area, California* (p. Vol. 588-137).

988   Glendora, CA.

989   Stephens, C. M., Marshall, L. A., Johnson, F. M., Lin, L., Band, L. E., & Ajami, H. (2020). Is

990   Past Variability a Suitable Proxy for Future Change? A Virtual Catchment Experiment.

991   *Water Resources Research*, *56*(2), e2019WR026275.

992   https://doi.org/10.1029/2019WR026275

993   Stephens, C. M., Marshall, L. A., Johnson, F. M., Ajami, H., Lin, L., & Band, L. E. (2022).

994   Spatial Variation in Catchment Response to Climate Change Depends on Lateral

995   Moisture Transport and Nutrient Dynamics. *Water Resources Research*, *58*(10),

996   e2021WR030577. https://doi.org/10.1029/2021WR030577

997   Sutton, M. A., Nemitz, E., Erisman, J. W., Beier, C., Bahl, K. B., Cellier, P., et al. (2007).

998   Challenges in quantifying biosphere-atmosphere exchange of nitrogen species.

999   *Environmental Pollution*, *150*(1), 125–139. https://doi.org/10.1016/j.envpol.2007.04.014

1000   Tague, C. L., & Band, L. E. (2004). RHESSys: Regional Hydro-Ecologic Simulation System—

1001   An Object-Oriented Approach to Spatially Distributed Modeling of Carbon, Water, and

1002   Nutrient Cycling. *Earth Interactions*, *8*(19), 1–42. https://doi.org/10.1175/1087-

1003   3562(2004)8<1:RRHSSO>2.0.CO;2

1004   Trenberth, K. E., Dai, A., Rasmussen, R. M., & Parsons, D. B. (2003). The Changing Character

1005   of Precipitation. *Bulletin of the American Meteorological Society*, *84*(9), 1205–1218.

1006   https://doi.org/10.1175/BAMS-84-9-1205

1007   Welter, J. R., Fisher, S. G., & Grimm, N. B. (2005). Nitrogen Transport and Retention in an Arid

1008   Land Watershed: Influence of Storm Characteristics on Terrestrial–aquatic Linkages.

1009   *Biogeochemistry*, *76*(3), 421–440. https://doi.org/10.1007/s10533-005-6997-7

1010   Winter, C., Nguyen, T. V., Musolff, A., Lutz, S. R., Rode, M., Kumar, R., & Fleckenstein, J. H.

1011   (2023). Droughts can reduce the nitrogen retention capacity of catchments. *Hydrology*

1012   *and Earth System Sciences*, *27*(1), 303–318. https://doi.org/10.5194/hess-27-303-2023

1013   Wu, Q., Yue, K., Ma, Y., Heděnec, P., Cai, Y., Chen, J., et al. (2022). Contrasting effects of

1014   altered precipitation regimes on soil nitrogen cycling at the global scale. *Global Change*

1015   *Biology*, *28*(22), 6679–6695. https://doi.org/10.1111/gcb.16392

1016   Ye, L., & Grimm, N. B. (2013). Modelling potential impacts of climate change on water and

1017   nitrate export from a mid-sized, semiarid watershed in the US Southwest. *Climatic*

1018   *Change*, *120*(1), 419–431. https://doi.org/10.1007/s10584-013-0827-z

1019   Yu, Q., Duan, L., Yu, L., Chen, X., Si, G., Ke, P., et al. (2018). Threshold and multiple

1020   indicators for nitrogen saturation in subtropical forests. *Environmental Pollution*, *241*,

1021   664–673. https://doi.org/10.1016/j.envpol.2018.06.001

1022   Zhu, Q., Castellano, M. J., & Yang, G. (2018). Coupling soil water processes and the nitrogen

1023   cycle across spatial scales: Potentials, bottlenecks and solutions. *Earth-Science Reviews*,

1024   *187*, 248–258. https://doi.org/10.1016/j.earscirev.2018.10.005

1025

1026